

# FINAL REPORT

## WELDABILITY OF HIGH ALLOYS

Contract Number 19X-SW314C

Submitted by: Iman Maroef and Glen R. Edwards  
Center for Welding, Joining, and Coatings Research  
Colorado School of Mines  
Golden, CO 80401-1887

Collaborators: Mark. D. Rowe and Steve Matthews (Haynes International Inc.)  
Stan David (Oak Ridge National Laboratory)

March, 2003

CSM



**Center for Welding, Joining  
and Coatings Researches**

Colorado School of Mines  
Golden. Colorado 80401

## TABLE OF CONTENT

EXECUTIVE SUMMARY .....	2
<b>1. The Effect of Silicon and Iron on the Weldability of Ni-Co-Cr-Si HR-160<sup>®</sup> Alloy</b> .....	<b>4</b>
1.1. Introduction.....	4
1.2. Materials and Experimental Procedures .....	4
1.2. Results.....	7
1.2.1. Solidification Cracking.....	7
1.2.2. Heat Affected Zone Cracking.....	19
1.3. Discussion.....	21
1.4. Conclusions.....	23
<b>2. The Effect of Artificial Aging on the HAZ Hot Cracking Susceptibility of Commercial HR-160<sup>®</sup> Superalloy</b> .....	<b>24</b>
2.1. Introduction.....	24
2.2. Hot Ductility Study of the As-received Commercial HR-160 alloy.....	24
2.3. Hot Ductility Study of the Artificially-Aged Commercial HR-160 alloy .....	27
2.4. Discussion.....	35
2.5. Conclusions.....	36

## EXECUTIVE SUMMARY

This report summarizes the research on current issues relevant to the welding metallurgy of HAYNES HR-160<sup>®</sup> superalloy\*. This research has been performed by the Colorado School of Mines' Center for Welding, Joining, and Coatings Research in collaboration with Haynes International, Inc. In this program, Haynes International provided both unique alloy, as well as supporting experimental data. In particular, Haynes International provided the vareststraint test data and material characterization of the as-received alloys. These data are included in this report for a complete description of the research. Haynes HR-160 superalloy was selected as the research topic because it has been proven applicable for many industries with harsh environmental operation, such as the electric power and the chemical processing industries. The current research aimed to enhance the application of this alloy by identifying the sources of problems associated with its fabrication and repair welding.

The research was comprised of two parts, each dealing with independent issues:

- the effect of silicon and iron on the solidification and HAZ hot cracking of the HR-160 alloy.
- the effect of artificial aging on the heat-affected zone (HAZ) hot cracking susceptibility of commercial HR-160 alloy.

The focus on silicon in Part One of this study was due to its major role in the sulfidation and oxidation resistance of the alloy at elevated temperatures. In an independent investigation by Haynes International, the sulfidation resistance was found to be significantly improved with silicon within the range of composition studied during this research, while the oxidation resistance was just slightly improved. The focus on iron was to explore the alloy's potential use for welding HR-160 to lower alloy steel. Part Two of the study was relevant to the repair welding of structures that have undergone extended use under elevated temperature conditions. This report is organized in two separate parts according to the two topics discussed above.

The solidification cracking susceptibility of the experimental alloys was evaluated with various weldability tests, including the vareststraint, the Sigma-jig, and the Gleeble hot ductility test. To understand the source of problems revealed by the weldability tests, differential thermal analysis and electron microscopic investigations were performed. The HAZ hot cracking susceptibility of the commercial HR-160 alloy, aged at 760 C and 780 C for 4000 hours each, was evaluated with the Gleeble hot ductility test. Fractographic and

---

\* HAYNES and HR-160 are trademarks of Haynes International Inc.

cross-sectional metallographic investigations of the samples were subsequently undertaken to identify mechanisms of fracture.

The solidification cracking susceptibility was increased by silicon and iron, with silicon having the predominant influence. The result implies that there is an upper limit to the addition of silicon to this alloy, in spite of the beneficial effect it provides for the corrosion resistance of the alloy at elevated temperatures. The detrimental effect of increasing silicon concentration was a corresponding increase in the solidification temperature range of the alloy. The exact role of iron in increasing the solidification cracking susceptibility was not clear. However, the effect of iron is not independent. There was an indication that the detrimental effect of iron was related to its interaction with silicon. Increased microsegregation of silicon to the interdendritic liquid during solidification, as induced by iron, was identified as a possible explanation for such a detrimental effect of iron. The current parameters and methodology employed to evaluate the weldability of this alloy were not sufficient to definitively explain the role of iron on the solidification cracking.

The evaluation of the HAZ hot cracking susceptibility of commercial HR-160 alloy led to a conclusion that artificial aging compromises the repair weldability. During simulated welding HAZ thermal cycles, the grain boundary liquation was reduced by at least 65 C as a consequence of the artificial aging. Artificial aging at 870 C was considered to pose more risk to cracking than aging at 760 C. Ductility recovery of the HR-160 alloy aged at 870 C was delayed about 50 C, while recovery of the alloy aged at 760 C was not significantly delayed. The Gleeble hot ductility test must be recognized as an augmented loading test that is best suited only to compare the hot cracking susceptibility of various materials. Hence, the results of these tests should be interpreted relative to a real welding experience on a specific material.

# 1. The Effect of Silicon and Iron on the Weldability of Ni-Co-Cr-Si HR-160<sup>®</sup> Alloy

## 1.1. Introduction

The purpose of this study was to investigate the effect of silicon and iron on the weldability of HAYNES HR-160<sup>® †</sup> alloy. HR-160 alloy is a solid solution strengthened Ni-Co-Cr-Si alloy. The alloy is designed to resist corrosion in sulfidizing and other aggressive high temperature environments. Silicon is added (~2.75%) to promote the formation of a protective oxide scale in environments with low oxygen activity. HR-160 alloy has found applications in waste incinerators, calciners, pulp and paper recovery boilers, coal gasification systems, and fluidized bed combustion systems.

HR-160 alloy has been successfully used in a wide range of welded applications. However, the alloy can be susceptible to solidification cracking under conditions of severe restraint. A previous study by DuPont, et al. [1] showed that silicon promoted solidification cracking in the commercial alloy. In earlier work conducted at Haynes, and also from published work by DuPont, et al., it was recognized that silicon segregates to the terminal liquid, creating low melting point liquid films on solidification grain boundaries. Solidification cracking has been encountered when using the alloy as a weld overlay on steel, and when joining HR-160 plate in a thickness greater than 19 millimeters (0.75 inches) with matching filler metal. The effect of silicon on the weldability of HR-160 alloy has been well documented, but the effect of iron is not well understood. Prior experience at Haynes has indicated that iron may be detrimental to the solidification cracking resistance of the alloy. Iron does not segregate to the terminal solidification product in nickel-base alloys, as does silicon [2], but iron may have an indirect or interactive influence on weldability. A set of alloys covering a range of silicon and iron contents was prepared and characterized to better understand the welding metallurgy of HR-160 alloy.

## 1.2. Materials and Experimental Procedures

### Materials

For this study, four HR-160 type experimental alloys with different target levels of silicon (2.3 and 3.9 %) and iron (0.10 and 4.0 %) were prepared. The experimental heats represent a [2 x 2] matrix of high and low silicon and iron. The heat 8727- 7- 7506 was included in this study to represent the standard commercial alloy. The chemical compositions of the experimental and commercial alloys are given in Table 1.

---

<sup>†</sup> HAYNES and HR-160 are trademarks of Haynes International Inc.

The experimental alloys were vacuum melted, cast into electrodes, then electroslag remelted into 102-mm (4-in.)-diam. ingots. The ingots were forged to 44.5 millimeters (1.75 inches), then further hot-rolled to 12.5-mm (0.5-in.) plate. The materials for vareststraint testing were prepared by hot rolling at 1021 C to 9.5-mm (0.375-in.) plate. The alloys were annealed at 1021 C for 20 minutes. and subsequently water quenched. Sigmajig specimens were taken from the hot rolled 12.5-mm (0.5-in.)-thick plate to be hot rolled to 2 millimeters (0.080 inches), then cold rolled to 1 millimeter (0.04 inches), followed by an anneal at 1100 C.

Table 1. Chemical compositions of the HR-160 type experimental and commercial alloys (wt.pct.)

Haynes Intl. Heat #	EN2799-9- 0894	EN2999-0- 0896	8727-7-7506	EN2899-9- 0895	EN3099-9- 0897
<b>Nominal Si &amp; Fe Content</b>	<b>2.3% Si 0.10% Fe</b>	<b>2.3% Si 4.0% Fe</b>	<b>2.8% Si 0.10 % Fe</b>	<b>4.0% Si 0.10% Fe</b>	<b>4.0% Si 4.0% Fe</b>
<b>Source</b>	<b>Commercial</b>	<b>Experimental</b>	<b>Experimental</b>	<b>Experimental</b>	<b>Experimental</b>
<b>Element</b>					
<b>B</b>	--	--	--	--	--
<b>C</b>	<b>0.062</b>	<b>0.061</b>	<b>0.05</b>	<b>0.062</b>	<b>0.065</b>
<b>Cb</b>	<b>&lt;.01</b>	<b>0.01</b>	<b>&lt;.050</b>	<b>0.01</b>	<b>0.01</b>
<b>Co</b>	<b>30.01</b>	<b>29.99</b>	<b>30.1</b>	<b>29.99</b>	<b>29.74</b>
<b>Cr</b>	<b>27.61</b>	<b>27.88</b>	<b>27.80</b>	<b>27.60</b>	<b>27.68</b>
<b>Fe</b>	<b>0.08</b>	<b>4.01</b>	<b>&lt;0.10</b>	<b>0.09</b>	<b>3.96</b>
<b>La</b>	--	--	--	--	--
<b>Mn</b>	<b>0.55</b>	<b>0.53</b>	<b>0.46</b>	<b>0.54</b>	<b>0.52</b>
<b>Mo</b>	<b>&lt;.01</b>	<b>&lt;.01</b>	<b>0.10</b>	<b>&lt;.01</b>	<b>&lt;.01</b>
<b>N</b>	--	--	--	--	--
<b>Ni</b>	<b>38.65</b>	<b>34.40</b>	<b>37.11</b>	<b>36.72</b>	<b>33.04</b>
<b>P</b>	<b>0.002</b>	<b>&lt;.002</b>	<b>0.002</b>	<b>0.005</b>	<b>0.006</b>
<b>S</b>	<b>&lt;.001</b>	<b>&lt;.001</b>	<b>0.007</b>	<b>&lt;.001</b>	<b>&lt;.001</b>
<b>Si</b>	<b>2.34</b>	<b>2.24</b>	<b>2.81</b>	<b>4.09</b>	<b>4.11</b>
<b>Ta</b>	--	--	--	--	--
<b>Ti</b>	<b>0.5</b>	<b>0.49</b>	<b>0.46</b>	<b>0.5</b>	<b>0.44</b>
<b>W</b>	<b>&lt;.01</b>	<b>&lt;.01</b>	<b>&lt;.10</b>	<b>&lt;.01</b>	<b>0.01</b>
<b>Zr</b>	--	--	--	--	--

### Solidification Cracking Tests

Longitudinal vareststraint tests were undertaken with a welding heat input of 2.2 kJ/mm and augmented strain of 1 percent. Each experimental alloy was tested in triplicate. Five replicate samples of the commercial HR-160 alloy were tested. The total crack length and maximum crack length were taken as indicators of the cracking susceptibility. Cracks were measured in the as-welded condition with a stereoscopic microscope.

Sigmajig testing of 50-mm × 50-mm coupons was also performed. As an indicator of cracking susceptibility, a threshold stress for crack initiation was measured. To determine the

threshold stress, the sigma jig test was performed over a range of applied stress, and the threshold stress was taken as the minimum stress to produce cracking. Hot cracks that formed in the fusion zone were measured under a stereoscopic microscope.

### Quantitative metallography

Metallographic samples were taken from welded specimens to analyze resulting microstructures. Samples were electrolytically etched at 6 volts using a solution of 5 grams oxalic acid dissolved in 95 milliliters of hydrochloric acid. The weld microstructures were initially analyzed using light optical microscopy. The volume percent of interdendritic eutectic constituent was measured metallographically using image analysis software. The average of 20 fields analyzed at 200x magnification was reported. Area percent on a metallographic cross-section was considered to be representative of the bulk volume percent.

### Differential Thermal Analysis

Differential thermal analysis (DTA) was performed with a Netsch Thermal Analyzer STA 409, using alumina as a reference. This analysis was intended to provide some thermodynamic basis to explain the trends in solidification cracking susceptibility of the different alloys. As a parameter for solidification susceptibility, the solidification temperature range (STR) assessed from DTA was determined. Alumina crucibles and lids, designed for differential scanning calorimetry (DSC), were used to increase sensitivity of the analysis. During initial analyses (DTA1), a sample mass of  $150 \pm 20$  milligrams was found sufficient for easy detection of reaction peaks. On-heating rate was determined to be  $0.083\text{C/s}$  ( $5\text{C/min.}$ ) to obtain near equilibrium solidus and liquidus temperatures. On the other hand, a rate of  $0.33\text{C/s}$  ( $20\text{C/min.}$ ) was selected for on-cooling analysis. In this way, reaction temperatures associated with non-equilibrium solidification can be measured. It was found from an alloy of interest that the liquidus temperature during cooling cycle varied as a result of unexplainable causes of undercooling. The variation was significant with the high cooling rate used in the initial analyses. To detect the liquidus more accurately during cooling cycle, the analyses were repeated (DTA2) with an initial cooling rate of  $0.05\text{C/s}$  to  $1250\text{C}$ , followed by a final cooling rate of  $0.33\text{C/s}$ . This final cooling rate was prescribed to allow easy detection of the terminal liquid reaction temperatures. The sample mass for DTA2 was determined to be  $300 \pm 30\text{mg}$ .

### Heat Affected Zone (HAZ) Hot Cracking Tests

Initial observation of the heat-affected zone cracking was taken from the vareststraint test samples. The vareststraint test is primarily meant to measure the resistance of alloys to solidification cracking in the fusion zone. However, heat-affected zone (HAZ) cracks will often be found in vareststraint test specimens of alloys that are susceptible to this type of cracking.

Susceptible alloys, identified in the vareststraint tests, were tested for hot ductility response with a Gleeble 1500 thermo-mechanical simulator. The Gleeble test subjects a sample to a

simulated weld thermal cycle, which is immediately followed by rapid tensile loading (65 mm/s). The first part of the hot ductility test was assessed during the heating cycle, and progressively done at increasing test temperature until the nil stress temperature was identified. Subsequently, the second part of testing was done during the cooling cycle that immediately following a heating cycle to a peak temperature. The peak temperature was the nil stress temperature (NST). It has been reported that tests utilizing the NST as a peak temperature discriminated to a greater degree than did those tests using a lower maximum temperature; e.g., NDT (nil ductility temperature).

Details of the testing followed the procedure proposed by Lundin, et al. [3]. In this procedure, the prescribed thermal cycle corresponds to that in 38-mm (1.5-in.)-thick stainless steel plate, welded with a heat input of 2.8 kJ/mm. A stabilizing time of 0.5 seconds was assigned in the thermal program before tensile loading, during both the heating and the cooling cycle. No annealing time was allowed at the peak temperature during on-cooling tests. Hot ductility was evaluated as the percent reduction in area. The ratio of ductility recovery (RDR) proposed by Lundin [4] was used as the indicator of HAZ susceptibility to hot cracking. The RDR is defined as the ratio of areas under the curve for on-cooling versus on-heating, measured from the on-heating peak ductility temperature to the NDT.

## **1.2. Results**

### **1.2.1. Solidification Cracking**

Results of the vareststraint and the sigmajig testing are plotted as a function of the silicon concentration in Figure 1. Data points of iron-rich samples are filled with black color to show the effect of iron for a given silicon concentration. Two criteria of solidification cracking, the average total crack length (TCL) and the maximum crack length (MCL) are presented in Figure 1. The MCL provides both a rapid quantitative means of assessing hot-cracking sensitivity and an indication of the relative hot-cracking temperature range. MCL has also been shown to correlate well with sigmajig threshold stresses and solidification temperature ranges (STR) [1,4,5]. Therefore, to discuss the solidification cracking susceptibility in the light of thermodynamic parameters such as the STR, MCL is the selected criterion. On the other hand, TCL is based on measurement of all cracks in a given sample and may provide additional information regarding the solidification cracking susceptibility of the alloy under investigation.

The results showed that both the vareststraint MCLs and sigmajig threshold stresses were in reasonable agreement, indicating the predominantly detrimental effect of silicon over that of iron. Both types of data showed that the cracking susceptibility increased with an increase in silicon content up to approximately the commercial HR-160 alloy's concentration (2.3 pct. Si). Then, the susceptibility leveled off at higher levels of silicon, within this test matrix. The detrimental effect of iron was considered significant at a low level of silicon, but was apparently overshadowed by silicon at a higher level of silicon.

In contrast to the MCL data, the TCL data showed that cracking susceptibility continuously increased with an increase in silicon, within the concentration established by the test matrix. Also, in contrast to the observation from the MCL and sigmajig criteria, the detrimental effect of iron on the susceptibility was increased at high silicon concentration when the TCL criterion was used.

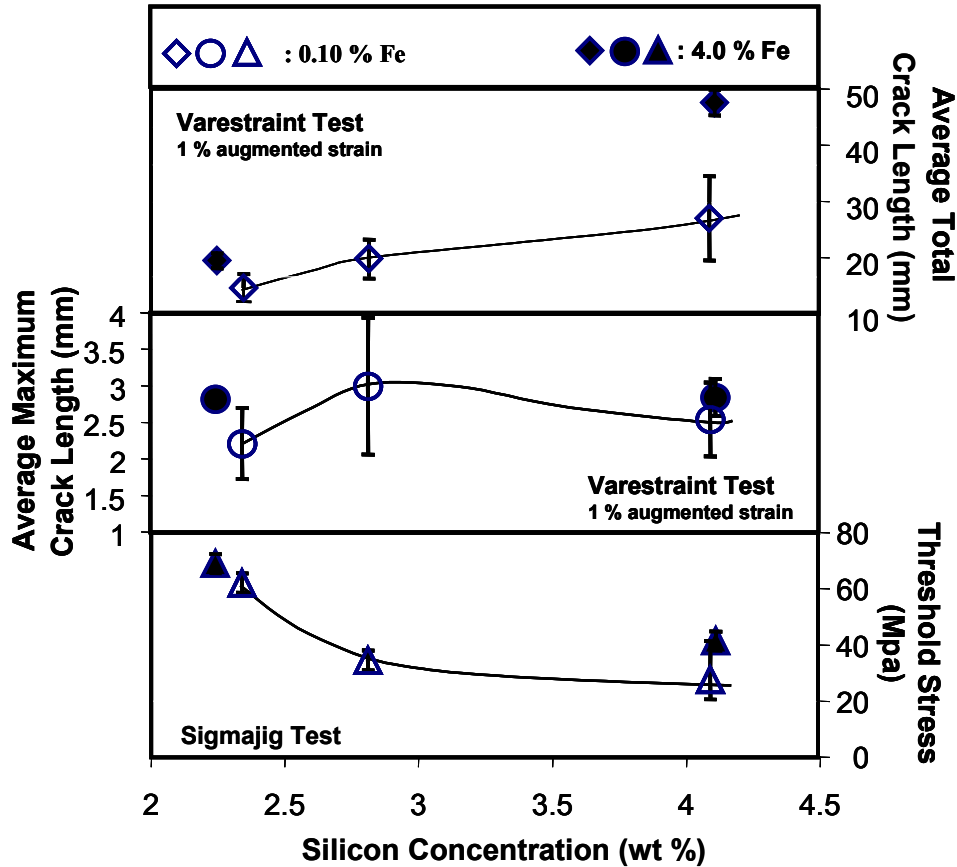


Figure 1. Solidification cracking susceptibility of the HR-160 type alloys with different silicon and iron concentrations.

The crack morphologies of three varestraint-tested weld metals (the commercial alloy and the two high-Si experimental HR-160 alloys) are shown in Figure 2 to Figure 4, along with micrographs exhibiting the morphology and distribution of the interdendritic eutectic products. There are larger numbers of cracks in the high-Si HR-160 alloys, suggesting that cracks can be initiated more easily in the high-Si alloys than in the low-Si alloys.

Cracks are smaller and more numerous in the high-Fe, high-Si alloy than those in the low-Fe, high-Si alloy. The effect of iron in the high-Si alloy appeared to be that of increasing the crack initiation sites, a phenomenon that might be associated with microstructure of the solidifying weld metal, such as the terminal liquid distribution along the grain boundaries. The amount and the liquid film network of interdendritic eutectic product are visibly less for

the commercial HR-160 alloy than for the two high-Si experimental alloys. Between the two high-Si alloys, the liquid film network of the eutectic product was roughly similar. It was realized that the solidification structure is complex, and that more than one cross-sectional view would be necessary for one to compare the quantity and distribution of the liquid film network created by thermal cycling a given material.

## Quantitative Metallography

Figure 5 shows the volume fraction of interdendritic eutectic as a function of the silicon concentration, both from the varestraint and the sigmajig test samples. The amount of eutectic product appears to be directly proportional to the silicon content of the alloy. Addition of iron at the levels tested had no measurable effect on the amount of eutectic liquid. In general, at small volume fractions of eutectic, hot cracking susceptibility increased with increasing eutectic product, due to an increase in the continuous terminal liquid that wets the grain boundaries. Above a threshold volume fraction (10 to 20 percent), sufficient liquid is available to back-fill and heal an incipient hot crack, leading to a reduction in cracking susceptibility. From the sigmajig and MCL data, the high-Si alloys may be approaching the quantity of eutectic product required for backfilling, but further data would be required to confirm that hypothesis. Also, the TCL data indicates that the eutectic volume fraction is smaller than the threshold value.

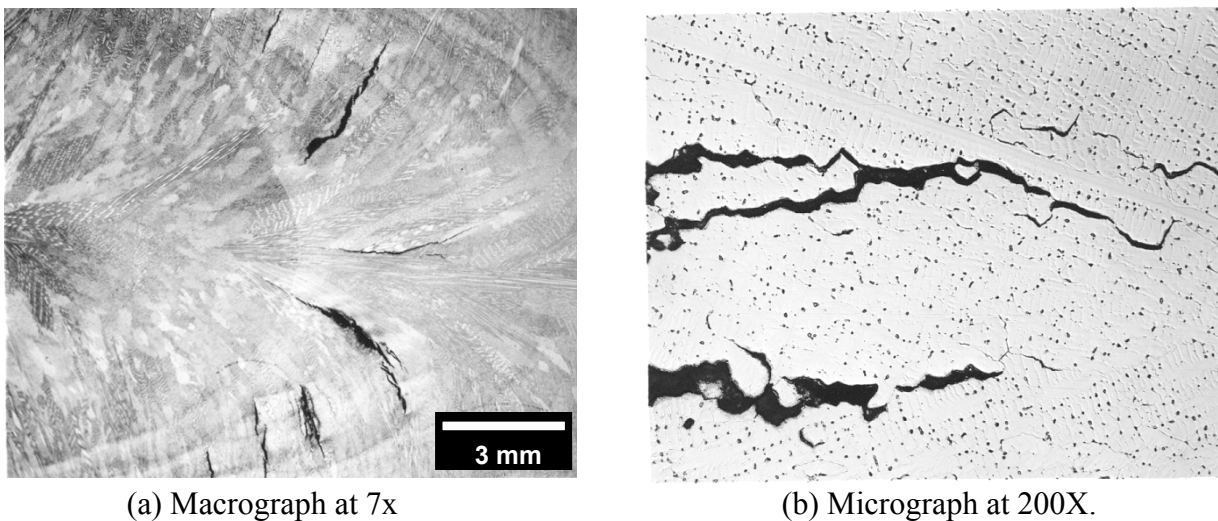
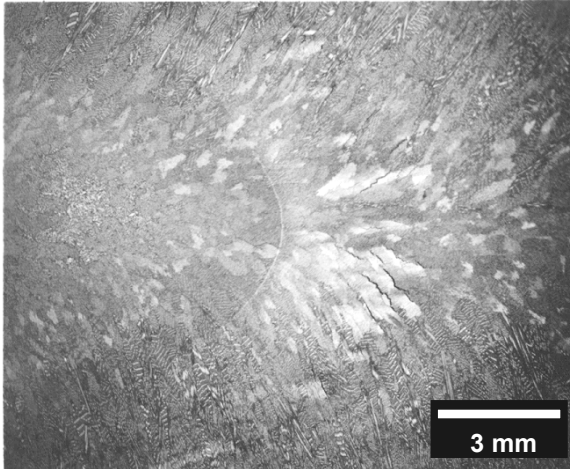


Figure 2. Longitudinal varestraint-induced solidification cracks in a commercial heat of HR-160 alloy.

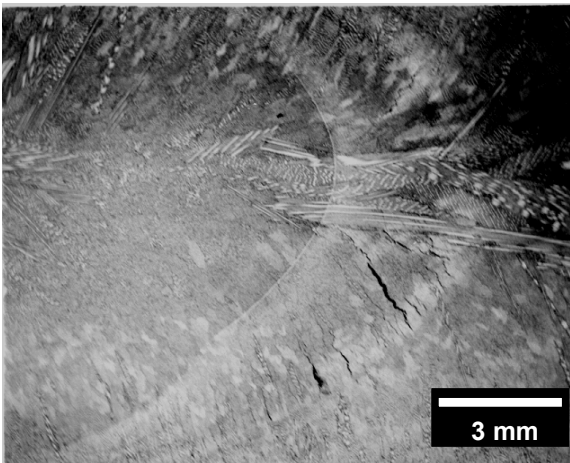


(a) Macrograph at 7x

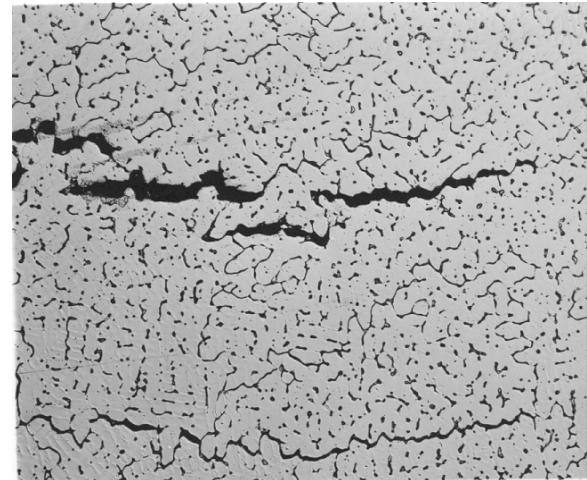


(b) Micrograph at 200X.

Figure 3. Longitudinal varestraint-induced solidification cracks in a 4.0-wt.-pct.-Si and 0.1-wt.-pct.-Fe HR-160 experimental alloy.



(a) Macrograph at 7x



(b) Micrograph at 200X.

Figure 4. Longitudinal varestraint-induced solidification cracks in a 4.0-wt.-pct.-Si and 4.0-wt.-pct.-Fe HR-160 experimental alloy.

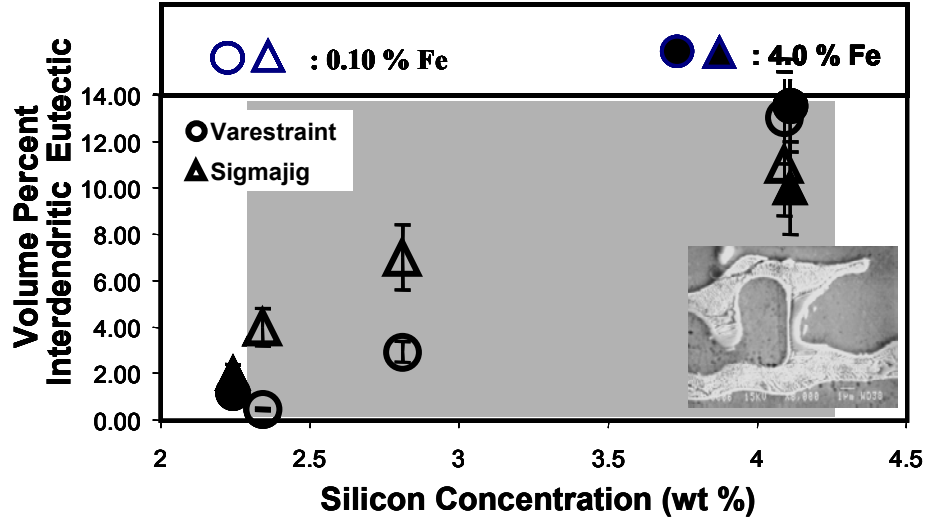


Figure 5. The quantity of interdendritic eutectic product in the weld metal of HR-160 type alloys with different silicon and iron concentrations, as measured from varestraint and sigmajig specimens.

### Secondary Electron Fractography

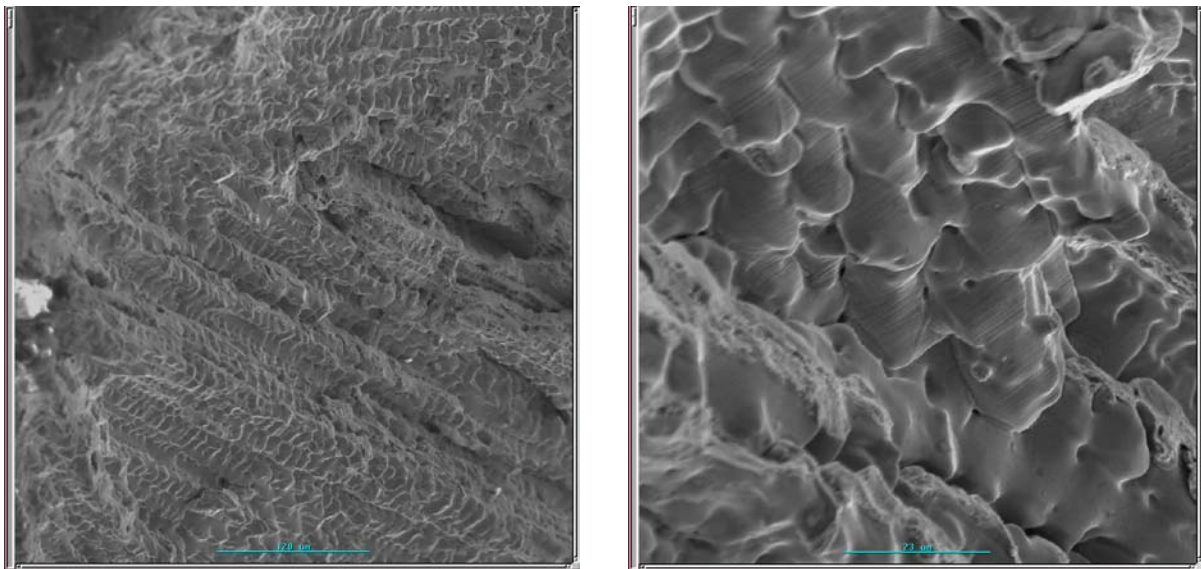
Details of the fracture surface of the three most susceptible alloys (the commercial alloy and the two high-Si experimental HR-160 alloys) are shown from Figure 6 to Figure 8. The fracture surfaces shown were documented from the varestraint test samples. The solidification cracks were opened with as much care as possible to prevent rubbing of the matching fracture surfaces. The fractographs shown in Figure 6 to Figure 8 were located immediately under the weld bead surface.

In the fracture surface of the commercial HR-160 alloy, as shown in Figure 6, classic dendritic structure is shown as evidence of the solidification cracking. The dendrites appeared to be predominantly columnar, with secondary dendrite arms not fully developed. Some plasticity, manifested as slip lines, is notable on the dendrite surfaces at high magnification. Due to the isolated morphology of the interdendritic eutectic product of the alloy (Figure 2), some plastic deformation would be necessary for the crack to propagate along the interdendritic path that was not the terminal liquid.

The fracture surface of the high-Si, low-Fe alloy is shown in Figure 7. The primary dendritic columns can be easily identified, one separated from another by a long span of secondary dendrite arms. Separation between the dendrites did not produce smooth fracture surfaces. At high magnification, many shear lips were visible, accompanied by small frozen droplets of liquid. These features imply that the some portion of the fracture process proceeded by a

viscoplastic mechanism. These observations suggest that the terminal liquid wet the solid dendrite quite well.

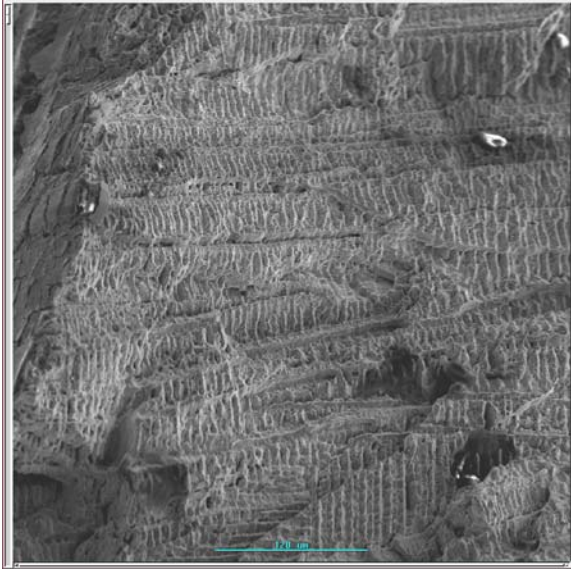
In contrast to the high-Si, low-Fe alloy, the fracture surface of the high-Si, high-Fe alloy (Figure 8) revealed a much more complex dendritic structure. The interdendritic liquid film appeared to be connected as a three-dimensional network. Such a complex network of the terminal liquid film was not as well revealed in the cross-sectional micrographs presented primarily in Figure 4. The dendrite surface also revealed traces of slip lines (as also seen on dendrites of the commercial alloy), implying that the crack did not propagate entirely through the terminal liquid. There are some islands of second phase on the dendrite surface, which should be interdendritic eutectic product. The isolation of these eutectic islands, accompanied with traces of slip lines on the dendrite surface (whenever uncovered by the eutectic product), indicates that the terminal liquid did not wet the solid dendrite completely.



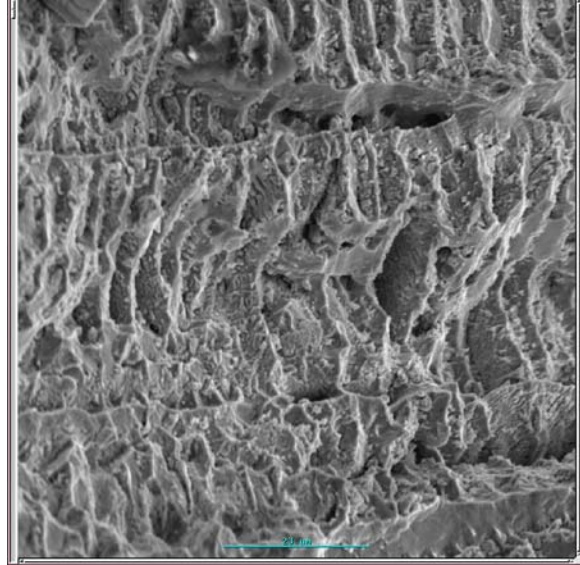
(a) Magnification at 200 X

(b) Magnification at 1000X.

Figure 6. SEM fractographs of commercial HR-160 weld metal.

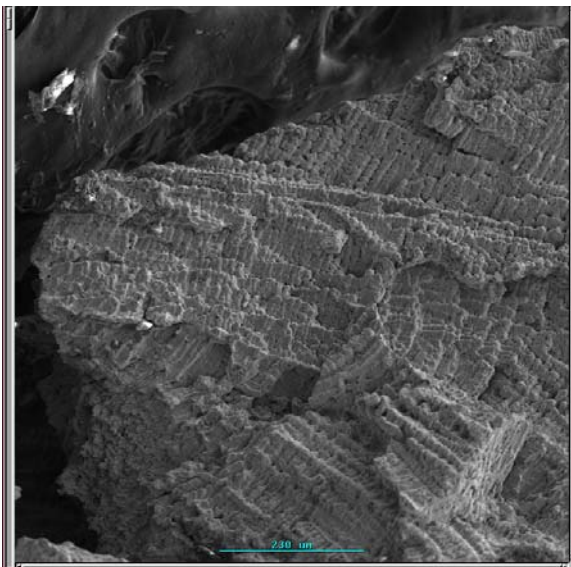


(a) Magnification at 200 X

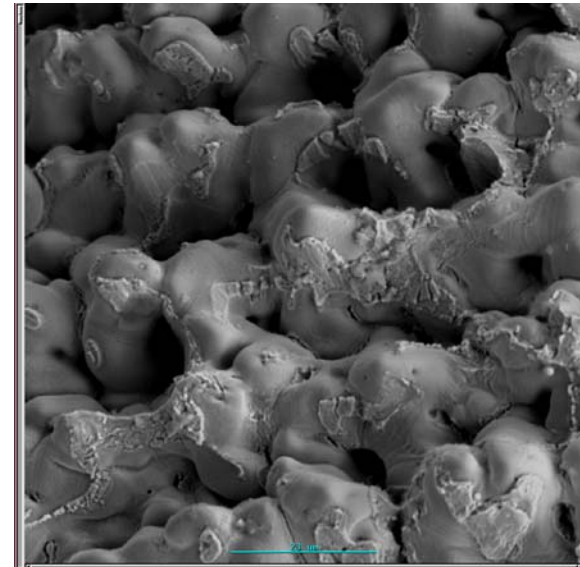


(b) Magnification at 1000X.

Figure 7. SEM fractographs of 4.0-wt.-pct.-Si and 0.1-wt.-pct.-Fe HR-160 type experimental weld metal.



(a) Magnification at 200 X



(b) Magnification at 1000X.

Figure 8. SEM fractographs of 2.3-wt.-pct.-Si and 4.0-wt.-pct.-Fe HR-160 type experimental weld metal.

## Partitioning Coefficients of Alloying Elements

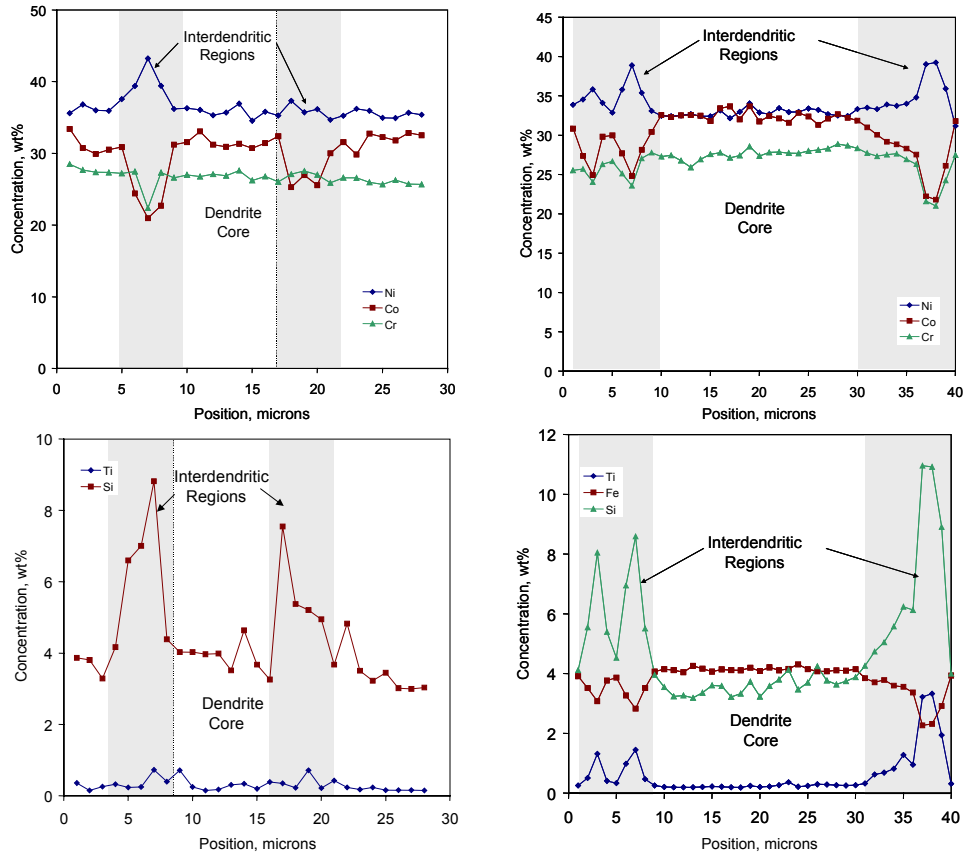
The complexity of the the solidification structures complicated the quantitative analyses of the interdendritic eutectic product. As an alternative, the degree of microsegregation of the major elements in the alloy can be used as a measure of the amount of terminal liquid. Microsegregation during solidification is governed by the partitioning coefficient ( $k$ ) of the particular elements in the alloy. Values of  $k$  for major elements can be estimated from an elemental profile across the solidification structure, and from basic solidification theory [1]. According to the Scheil equation, local equilibrium between solid and liquid is formulated as:

$$C_s = k C_o (1 - f_s)^{k-1} \quad [1a]$$

$$C_l = C_o (f_l)^{k-1} \quad [1b]$$

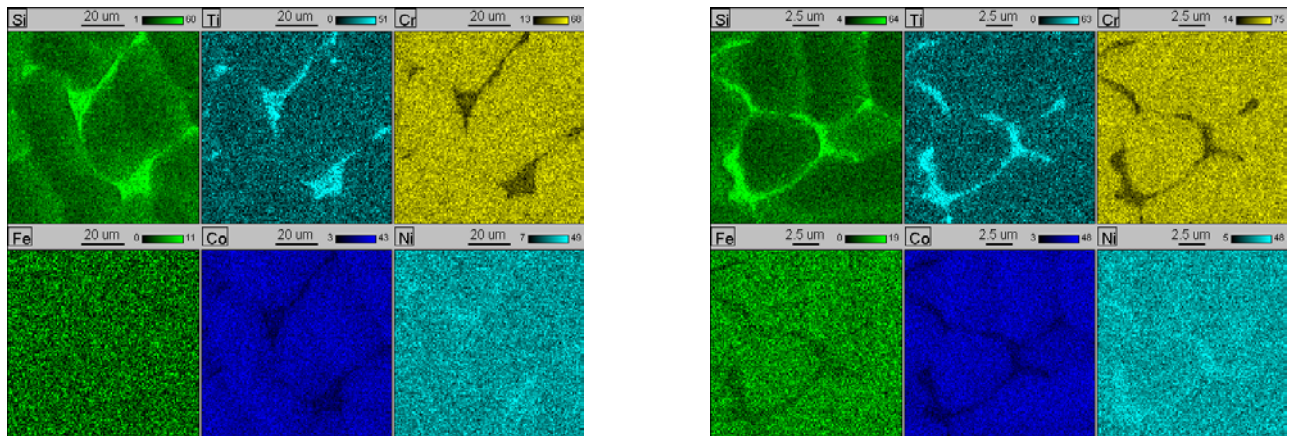
Where  $k$  is the equilibrium partitioning coefficient, defined as the ratio of solid to liquid composition at any temperature,  $C_s$  and  $C_l$  are the solid and liquid compositions at the fractions of phases presents ( $f_s$  or  $f_l$ ), and  $C_o$  is the nominal composition. This relation assumes that dendrite tip curvature effects and solid-state diffusion are negligible, that thermodynamic equilibrium is maintained at the solid/liquid interface, and that diffusion of elements in the liquid is very fast. According to this definition, an element with a low  $k$  value segregates strongly to the terminal liquid phase. Assuming invariant chemical composition of the eutectic (terminal liquid  $C_l$  is equal to eutectic composition) within an alloy system, from equation 1b,  $k$  can be related to the amount of terminal liquid ( $f_l$ ). The lower the  $k$  value, the larger the amount of terminal liquid. The  $k$  values for the two high-Si alloys have been assessed from elemental concentration profiles across the solidification structure, as shown in Figure 9. These profiles were measured by wave-length dispersive spectroscopy (WDS). During the initial stage of solidification ( $f_s = 0$ ), Equation 1a becomes  $C_s = kC_o$ . Using the concentration of the dendrite cores as  $C_s$  and knowing  $C_o$  of the alloys, the apparent  $k$  values for selected elements were calculated for the two high-Si alloys and are listed in Table 2. It should be emphasized that these apparent  $k$  values were just an approximation, and that they are subject to inaccuracies originating from inexact location of the plane of the cross-section relative to the axis of the dendrite core. Also, back-diffusion of the alloying elements during solidification has been recognized as another source of inaccuracy in assessing the apparent  $k$  values.

Taking silicon as the major segregating element, the effect of iron is expected to slightly increase the amount of terminal liquid, and thus the solidification cracking susceptibility of the high-Si alloys, by lowering the apparent  $k$  values. The tendency for elemental microsegregation of the two alloys, as measured from their apparent  $k$  values, appeared to agree quite well with the X-ray elemental dot mapping shown in Figure 10. Included in Table 2 are apparent  $k$  values assessed by DuPont [1] from weld overlay of HR-160 superalloy on 2.5Cr-1Mo steel. With even higher iron content, it was shown that the  $k$  value of silicon was further decreased.



(a) 4.0 wt. pct. Si and 0.1 wt. pct. Fe      (b) 4.0 wt. pct. Si and 4.0 wt. pct. Fe

Figure 9. Elemental distribution within the dendrite cores and the terminal liquid of experimental HR-160 alloy weld metals.



(a) 4.0 wt. pct. Si and 0.1 wt. pct. Fe

(b) 4.0 wt. pct. Si and 4.0 wt. pct. Fe

Figure 10. Elemental X-ray dot mapping of the solidification structure of HR-160 experimental weld metals.

Table 2. Apparent values of initial partitioning coefficients,  $k$ , of selected elements in high-Si HR-160 experimental alloy weld metal, as well as in HR-160 overlay weld on 2.25Cr-1Mo steel (Dupont [1]).

Element	4.0% Si - 0.10 % Fe			4.0%Si - 4.0%Fe			Weld Overlay (DuPont)		
	Co	Cs @ fs =0	k	Co	Cs @ fs -0	k	Co	Cs @ fs -0	k
Iron	0.09	ND	NA	3.96	4.11	1.04	32.91	37.53	1.14
Nickel	36.72	35.44	0.97	33.04	32.48	0.98	25.83	23.79	0.92
Chromium	27.60	26.41	0.96	27.68	27.84	1.01	19.22	19.02	0.99
Cobalt	29.99	30.91	1.03	29.74	32.34	1.09	20.01	21.54	1.08
Silicon	4.09	3.92	0.96	4.11	3.45	0.84	1.93	1.02	0.53
Titanium	0.5	0.24	0.48	0.44	0.22	0.50	0.34	ND	NA

## Differential Thermal Analysis

Figure 11 exhibits the DTA1 results for the commercial HR-160 alloy, containing both the on-heating and on-cooling thermogram curves. During heating, the sample exhibits a solidus temperature of approximately 1300 C (determined as the onset of a detectable difference in the endothermic part of the curve) and reaches the liquidus temperature at 1370 C (determined as the peak of the endothermic reaction). The near equilibrium melting range was 70 C, similar to the result reported earlier by DuPont [1]. Upon solidification, the alloy exhibited a large exothermic peak at an under-cooled temperature of 1340 C, which corresponded to the formation of the primary dendrites. Such an undercooling also occurred at the analyses for the other HR-160 experimental alloys. Solidification was completed with a terminal liquid exothermic reaction at 1150 C. Due to this large undercooling, the solidification temperature ranges 1 (STR1) for the alloys were taken as the difference between the on-heating liquidus temperature and the on-cooling terminal liquid reaction temperature. When considering the epitaxial growth during weld metal solidification, one could expect the required undercooling to be much smaller. However, the liquidus temperatures during heating might not be very accurate due to the presence of high melting oxides, depending on their volume fraction. As a complementary data, the solidification temperature ranges 2 (STR2) were also calculated, from the difference between the on-cooling liquidus and the terminal liquid temperatures, assessed during DTA2 analyses described in the experimental procedure. For the HR-160 commercial alloy, the STR1 and STR2 were 219 C and 212 C, respectively. Table 3 lists the reaction temperatures and the STR values of the alloys.

As shown in Figure 12, the melting and solidification temperatures of the two low-Si alloys were similar. An apparent difference in the DTA curves is associated with a large undercooling that occurred with the low-Si, low-Fe alloy. The terminal liquid reactions were not detected with the test parameters used in the current DTA. The amount of interdendritic eutectic in these alloys, shown in Figure 5, might be too small for the samples to give sufficient thermal fluctuation to the DTA apparatus. The final solidification temperature could not be accurately determined because standard procedure to determine a finish temperature of a reaction in DTA usually applies only to single-temperature exothermic or endothermic reactions. However, a reduction in STR due to lower silicon concentration could be observed. In addition, there was no measurable effect caused by the different concentration of iron within the two low-Si alloys. However, the observed increase in the susceptibility of solidification cracking, both from the vareststraint and the sigmajig data, implied that STR was not the only factor to cause higher susceptibility to solidification cracking in the high-Fe, low-Si HR-160 alloy.

The DTA curves from the high-Si alloys were also similar, as shown in Figure 13, with their terminal liquid reactions easily detected. The fact that the STR1/STR2 of both alloys, 215/205 C and 211/200 C, were not significantly different was consistent with the small difference in the MCL and the sigmajig threshold stress of the two alloys. In other words, from the STR standpoint, iron is not expected to increase the solidification cracking susceptibility of the high-Si HR-160 alloy.

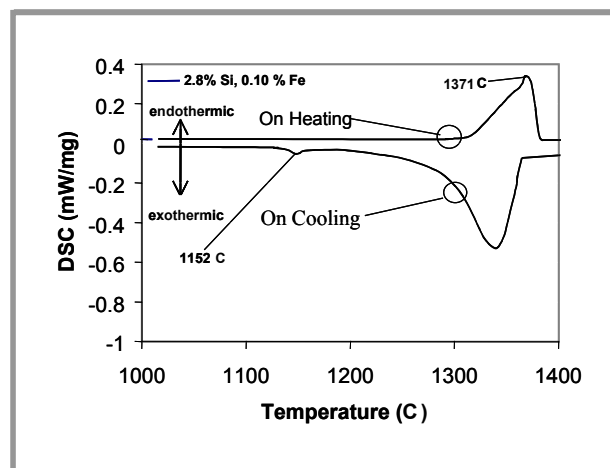


Figure 11. DTA thermogram of the commercial HR-160 alloy during melting at 0.083 C/s and solidification at 0.33 C/s.

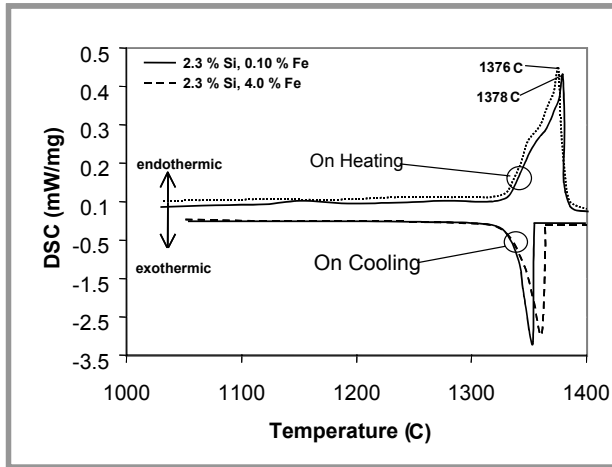


Figure 12. DTA thermogram of low-Si HR-160 type experimental alloys during melting at 0.083 C/s and solidification at 0.33 C/s.

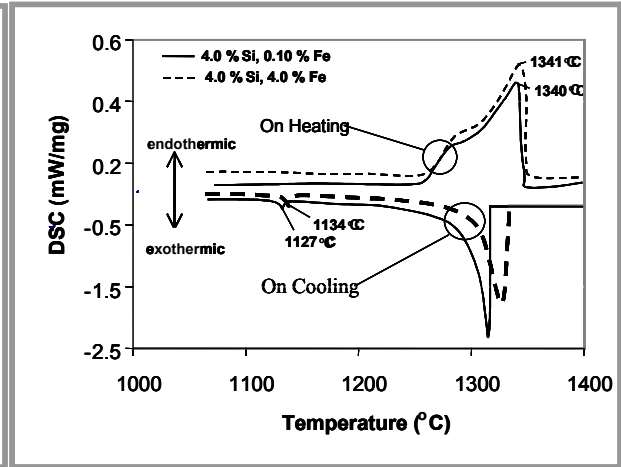


Figure 13. DTA thermogram of high-Si HR-160 type experimental alloys during melting at 0.083 C/s and solidification at 0.33 C/s.

Table 3. Results of Differential Thermal Analysis and Apparent Solidification Temperature Ranges.

Alloy	On Heating Liquidus (C) *	On Cooling Liquidus (C) **	Terminal Liquid (C) ***	Solidification Temp. Range STR1 (C)	Solidification Temp. Range STR2 (C)
2.3%Si, 0.1%Fe	1378 ± 5		ND	ND	ND
2.3%Si, 4.0%Fe	1376 ± 5		ND	ND	ND
2.8%Si, 0.1%Fe	1371 ± 5	1364 ± 5	1152 ± 5	219 ± 5	212 ± 5
4.0%Si, 0.1%Fe	1340 ± 5	1330 ± 5	1125 ± 5	215 ± 5	205 ± 5
4.0%Si, 4.0%Fe	1341 ± 5	1330 ± 5	1130 ± 5	211 ± 5	200 ± 5

ND = Not Detected

STR1 = On Heating Liquidus Temp. — Terminal Liquid Temp., values from DTA1.

STR2 = On Cooling Liquidus Temp. — Terminal Liquid Temp., values from DTA2.

\* : values were assessed from DTA1 with heating rate of 0.083 C/s to 1500 C and cooling rate of 0.33 C/s

\*\* : values were assessed from DTA2 with heating rate of 0.33 C/s to 1500 C and initial cooling rate of 0.05 C/s to 1250 C, followed by final cooling rate of 0.33 C/s for detection of terminal liquid temperature.

\*\*\* : values for terminal liquid temperature was an average of values assessed with DTA1 and DTA2.

### 1.2.2. Heat-Affected Zone Cracking

In the vareststraint test, the commercial HR-160 alloy and the high-Si HR-160 experimental alloys displayed a measurable amount of HAZ cracking, while the low-Si alloys did not. It is worth mentioning that in the experience of Haynes International, HAZ cracking has not been observed in engineering components fabricated from the commercial HR-160 alloy. The microstructure associated with HAZ cracking in the high-Si, high-Fe alloy can be seen in Figure 14. In the base material far from the HAZ, round particles were observed. These particles may be the silicon-rich G phase that formed during solidification of the ingot, then was broken up by hot working, but was not completely dissolved. The silicon-rich G phase  $[(\text{Ni}, \text{Co})_{16}(\text{Ti}, \text{Cr})_6(\text{Si})_7]$  is known to form during solidification of the HR-160 alloy [1]. These silicon-rich particles are not typically observed in the commercial alloy.

Also shown in Figure 14 are HAZ cracks that extended several grain diameters away from the fusion boundary. Solidified eutectic liquid was plainly visible in the cracks. The liquid may have originated from the fusion zone and penetrated along the grain boundaries, or it may have come from constitutional liquation of the primary particles, which were abundant in the high-Si alloys. The dark islands contained within the last row of equiaxed grains adjacent to the fusion boundary in the high silicon alloy of Figure 14 may be primary particles that have undergone constitutional liquation.

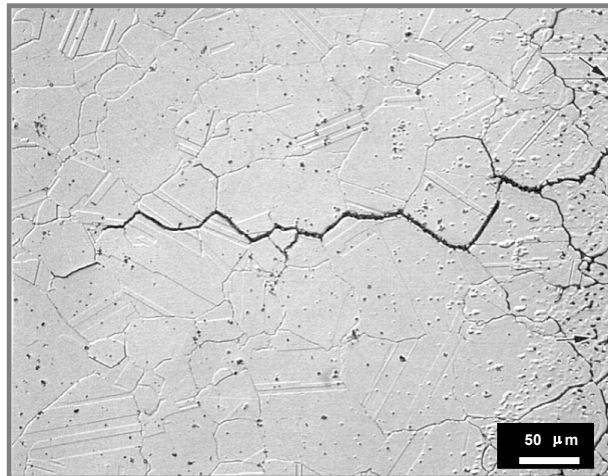


Figure 14. Longitudinal vareststraint-induced HAZ cracks in 4.0-wt.-pct.-Si , 4.0-wt.-pct.-Fe HR-160 experimental alloy

Based upon observations of HAZ cracks in the vareststraint tests, only three out of the five alloys investigated were subjected to the Gleeble hot ductility test. These alloys were the two high-Si heats and the commercial HR-160 alloy. The Gleeble hot ductility data for three alloys under investigation are shown in Figures 15 to 17, with their corresponding RDR values displayed.

Figure 15 shows that there was a good hot ductility recovery upon cooling for the commercial HR-160 alloy. The ductility turned to zero when the temperature reached 1240 C, which was then almost immediately recovered during the on-cooling tests. A small nil ductility range (NDR) was possible, but difficult to determine. The limited availability of samples did not allow for narrower temperature intervals within the vicinity of NDT to be tested. A mid-temperature reduction of ductility recovery occurred at temperatures below 1175 C, resulting in a RDR value for the alloy of 87 percent.

Figures 16 and 17 demonstrated that the hot ductility responses of the two high-Si HR-160 experimental alloys were similar. Both had a nil ductility temperature (NDT) of 1080 C and a nil ductility range (NDR) of approximately 25 C (relative to NDT). The NDT in these alloys was expected to be lower than that of the commercial alloy because the wrought microstructures of the high-Si alloys exhibited large numbers of primary particles that likely underwent constitutional liquation, as was indicated in Figure 14. The RDR values for both alloys (71 and 73 pct.) were also very similar. Such a similarity in the hot ductility responses of the two high-Si alloys was consistent with the similarities observed in the solidification cracking susceptibility of the two alloys. Recall that the vareststraint MCL and the sigmajig threshold stress values (considering the experimental errors) suggested similar cracking susceptibility.

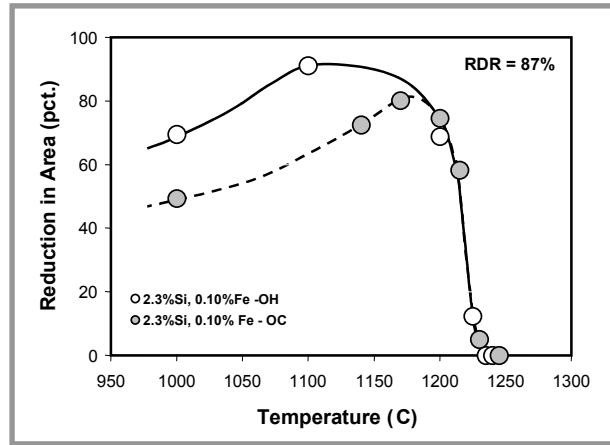


Figure 15. Gleeble hot ductility data for the HR-160 commercial alloy.

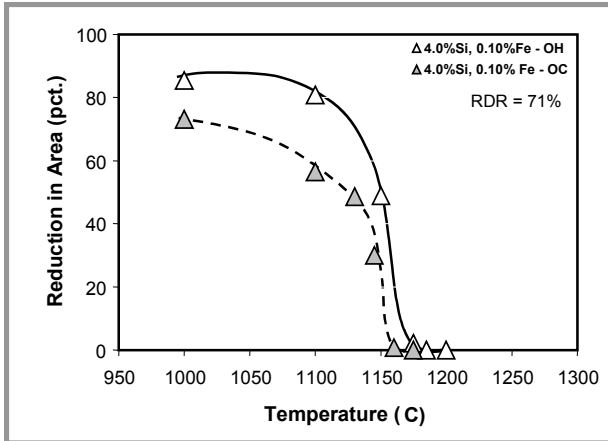


Figure 16. Gleeble hot ductility data for HR-160 experimental alloy with target concentrations of 4.0 wt. pct. Si and 0.10 wt. pct. Fe.

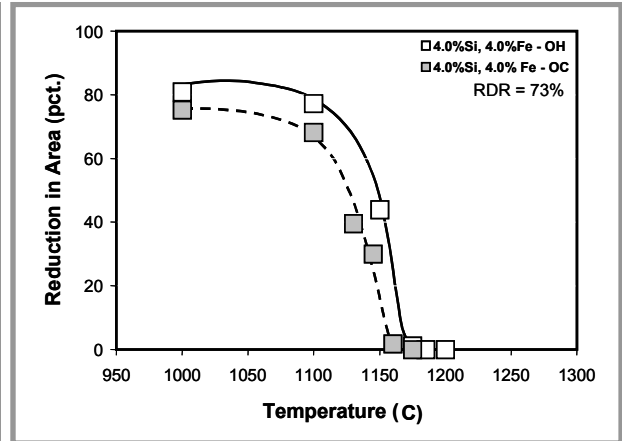


Figure 17. Gleeble hot ductility data for HR-160 experimental alloy with target concentrations of 4.0 wt. pct. Si and 4.0 wt. pct. Fe.

### 1.3. Discussion

Solidification cracking susceptibility is known to be controlled by the solidification temperature range (STR) and by the amount and distribution of interdendritic terminal liquid. The larger the value of STR or the larger the amount of terminal liquid (for values less than 10-12 pct.), the higher is the solidification cracking susceptibility of the alloy. The DTA measurements of the alloys revealed that silicon was the predominant element to govern the STR, although the correlation between the STR and silicon content was not linear. Iron did not seem to increase the STR of the high-Si HR-160 alloy. Furthermore, the MCL values of the varestraint test, as well as the sigma jig threshold stresses, appeared to correlate reasonably well with the corresponding STR values, as has been shown to be the case for other alloy systems by other investigators.

From the partitioning coefficient calculations, the effect of iron in high-Si HR-160 alloys is expected to be detrimental, because the lower  $k$  values associated with increased iron content should create larger fractions of terminal liquid. Assuming that the  $k$  value governs the amount of interdendritic terminal liquid (eutectic product), a higher value of TCL in the high-Si, high-Fe HR-160 alloy can be explained by the larger volume of interdendritic terminal liquid available to initiate multiple cracks during solidification. On the other hand, the surface tension of the liquid-solid interface, which may be related to the  $k$  values, also influences the solidification cracking susceptibility. A low value of surface tension would favor wetting of the solid dendrite by the terminal liquid, resulting in increased solidification cracking susceptibility by creating continuous networking of the terminal liquid film. In this standpoint, an increase in  $k$  value may increase cracking susceptibility by enhancing the liquid film network. It is anticipated that the wettability on the solid-liquid interface would be improved because the compositional difference between solid and liquid is less when the  $k$

value increases. The fracture surface of the high-Si, low-Fe HR-160 alloy in Figure 7, with the presence of apparent viscoplastic shear lips and liquid droplets, suggested that an increased  $k$  value enhanced the terminal liquid film network. Between the two opposite effects related to a  $k$  value, the amount of terminal liquid (due to low  $k$  values) is considered to be most significant factor related to solidification cracking.

The results of weldability tests showed that the MCL values of the vareststraint tests and the threshold stresses of the sigmajig tests gave the same indication of crack susceptibility for the various alloys. The discrepancies between the TCL values from the vareststraint tests and the threshold stresses from the sigmajig tests are still not completely understood. An unresolved concern is whether many fine cracks (a higher TCL value) poses a higher risk for weld joint degradation, even though a crack with the size of the MCL value has already formed. It is realized that each test has its own limitation and advantages, and the alloys of interest may not be adequately evaluated by these tests. The sigmajig test has been shown to be marginally adequate at low values of threshold stress. Previous experimental work [6], supported by finite element calculations, revealed that “free-stress” (zero preset loading) specimens could crack during welding solidification, but resisted cracking at moderate levels of pre-set loading. It was found that, due to the peculiarity of the sigmajig set-up, the free-stress condition lacks sample restraint. During heating, the sample can easily expand in all directions, causing significant tensile stress in the transverse direction during the cooling cycle. A minimum level of preset load is required to prevent such a free expansion. Hence, it is difficult to assess threshold stress values accurately for materials with relatively low threshold stress, as are HR-160 alloys. The susceptibility of HR-160 superalloy to solidification cracking has been shown to be higher than those of stainless steel and Alloy 718 [1].

The problem associated with the vareststraint test is finding the proper range of augmented strain. A complete evaluation using the vareststraint test involves straining the weld samples at several differing augmented strains. Starting with the lowest strain, the MCL value will continue to increase with additional strain until it levels off to a maximum value at a threshold value of augmented strain. Previous study of the commercial HR-160 alloy found that the MCL values leveled off at an augmented strain of approximately 1.5 percent. These maximum MCL values are the ones that correlated well with STR values. The use of 1 percent strain in this study is considered acceptable because the MCL values were quite close to the maximum for this alloying system. It was reasonable to find that the two high-Si HR-160 alloys displayed maximum MCL values similar to that of the commercial alloy. However, it is not clear what augmented strain level was best for measuring the maximum MCL values of these alloys. It is anticipated that the two high-Si HR-160 alloys would reach maximum MCL at a lower augmented strain than 1 percent, accompanied by a reduced average TCL, particularly for the high-Si, high-Fe HR-160 alloy. The crack susceptibility of the HR-160 alloys caused by increasing iron concentrations could not be defined by using only 1 percent augmented strain. Since the STR values correlated well with MCL values, the degree of microsegregation as measured by the apparent  $k$  values of the alloys could be used to explain the high TCL values in the high-Si, high-Fe HR-160 alloy. A test at lower augmented strain will be necessary to clearly identify whether iron additions increase the difficulty of welding with high-Si HR-160 alloys.

## 1.4. Conclusions

1. Within the tested levels of alloying addition, both silicon and iron additions proved to increase the susceptibility of the alloy to solidification cracking, with silicon having the predominant influence.
2. The solidification temperature ranges (STR) of the alloys depended upon the silicon content, with Fe having no measurable effect. The measured STRs from the various alloys correlated reasonably well with the MCL values of the varestraint test and the threshold stress values of the sigma-jig test.
3. The apparent k value of the high-Si HR-160 superalloy was increased by the addition of iron. Assuming that the k value governs the amount of interdendritic terminal liquid, a higher value of TCL in the high-Si, high-Fe HR-160 superalloy can be explained by the larger volume of interdendritic terminal liquid available to initiate cracks during solidification. Complexity of the solidification structure caused inaccuracy in the quantitative metallographic analysis of the eutectic volume fractions.
4. The two high-silicon alloys exhibited a lower ratio of ductility recovery (RDR) than the commercial HR-160 alloy in the Gleeble test, indicating a lower resistance to HAZ hot cracking for the high-Si HR-160 superalloys.
5. No significant difference was detected between the hot ductility responses of the two high-Si alloys (low and high Fe), implying that iron did not significantly affect the HAZ hot cracking susceptibility of the modified HR-160 superalloys.

## **2. The Effect of Artificial Aging on the HAZ Hot Cracking Susceptibility of Commercial HR-160<sup>®</sup> Superalloy**

### **2.1. Introduction**

Repair of commercial Haynes HR-160<sup>®</sup> superalloy ‡ components after prolonged high temperature use is a critical issue for the application of this alloy. To respond to this concern, hot ductility of artificially aged commercial HR-160<sup>®</sup> alloys has been studied. Two aging schedules were selected: 760C and 870C for 4000 hrs. The HAZ cracking susceptibility of the various alloy conditions was evaluated through the standard Gleeble hot ductility testing.

The Gleeble test subjects a sample to a simulated weld thermal cycle, which is immediately followed by rapid tensile loading (65 mm/s). The first part of the hot ductility tests was assessed during the heating cycle, and progressively done at increasing test temperature until the nil stress temperature was identified. Subsequently, the second testing was done during the cooling cycle that immediately followed a heating cycle to a peak temperature. The peak temperature was the nil stress temperature (NST). It has been reported that tests utilizing the NST as a peak temperature discriminated to a greater degree than did those tests using a lower maximum temperature; e.g., NDT (nil ductility temperature).

Details of testing followed the procedure proposed by Lundin, et al. [3]. In this procedure, the prescribed thermal cycle corresponds to that in 38-mm-(1.5-in.) thick stainless steel welded with a heat input of 2.8 kJ/mm. A stabilizing time of 0.5 seconds was assigned in the thermal program before tensile loading, during both the heating and the cooling cycle. No annealing time was allowed at the peak temperature during on-cooling tests. Hot ductility was evaluated as the percent reduction in area. The ratio of ductility recovery (RDR) proposed by Lundin [4] was used as the indicator of HAZ susceptibility to hot cracking. The RDR is defined as the ratio of areas under the curve for on-cooling versus on-heating, measured from the on-heating peak ductility temperature to the NDT.

### **2.2. Hot Ductility Study of the As-Received Commercial HR-160 alloy**

As a reference, the as-received commercial HR-160 alloy was the first to be evaluated for its hot ductility response. This alloy is designed to be solid solution strengthened; hence, the hot-rolled microstructure, shown in Figure 18, is a typical condition for its initial use. A small number of precipitates were observed in the as-received condition, as a consequence of incomplete homogenization both in the annealing and the hot-rolling processes. The average grain size was approximately 50  $\mu\text{m}$ , and some grains contained annealing twin boundaries.

---

‡ HAYNES and HR-160 are trademarks of Haynes International Inc.

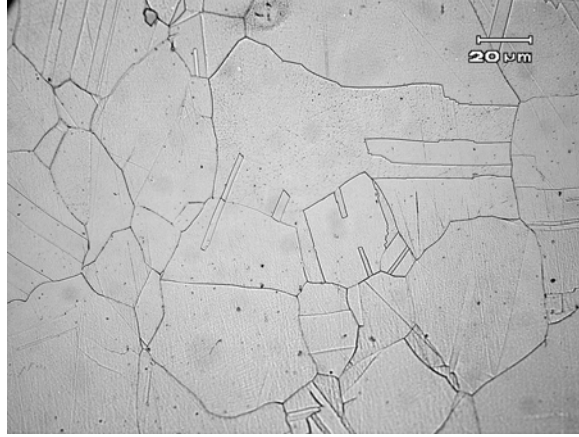


Figure 18. Optical micrograph of the as-received commercial Haynes HR-160 alloy.

The hot ductility response of the as-received commercial HR-160 alloy is shown in Figure 19a, accompanied by values of the corresponding engineering fracture stresses in Figure 19b. The hot ductility recovery of the as-received commercial HR-160 alloy was good. Upon heating, the ductility diminished when the temperature reached 1240C, which was then almost immediately recovered during the subsequent on-cooling cycles. A small nil ductility range (NDR) was possible, but difficult to determine. The limited availability of samples did not allow for narrower temperature intervals within the vicinity of NDT to be tested. A mid-temperature reduction of ductility recovery occurred at temperatures below 1175C, resulting in a RDR value of the alloy of 87 percent. The engineering stresses associated with tensile loading during the cooling cycles were less than those values associated with the heating cycles only. This finding implies irreversible microstructural change occurred during the course of HAZ simulated thermal cycles that reduced the strength of the alloy. The simulated HAZ thermal cycle is defined as the thermal cycle that includes heating to the peak temperature, then immediately cooling the specimen.

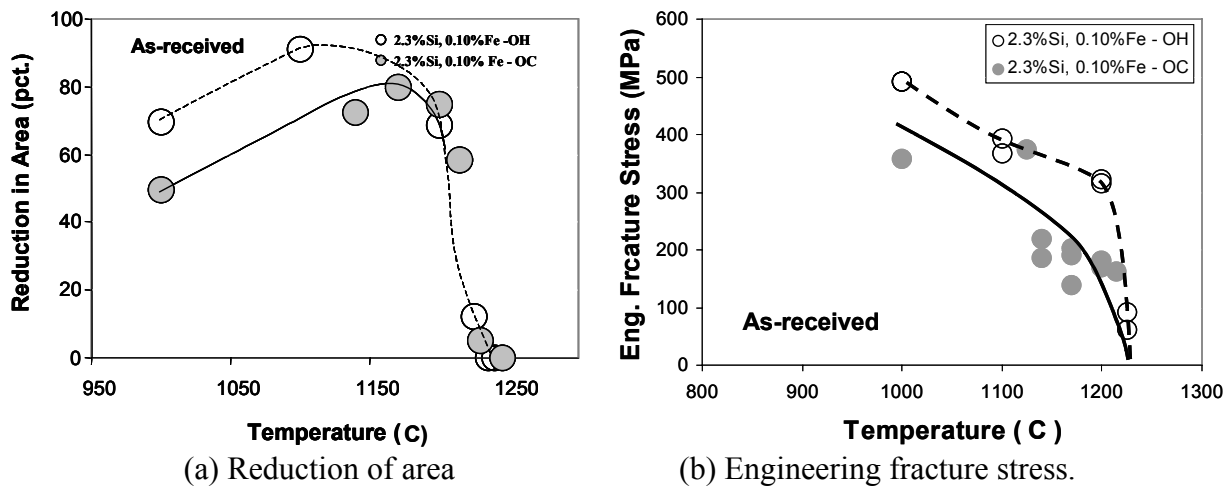


Figure 19. Gleeble hot ductility data for the commercial HR-160 alloy, in the as-received condition

Fractographs of selected samples are shown from Figure 20 to Figure 22. When fractured during the heating cycle at 1000 C, the sample appeared to fracture with a mixed mode of transgranular and intergranular microvoid coalescence. At the peak heating cycle temperature of 1240 C, grain boundary liquation was verified as the mode of failure above the NDT temperature. Finally, after the fully simulated HAZ thermal cycle (heated up to peak temperature of 1240 C and cooled down to 1000 C) the fracture surface contained transgranular, coalesced microvoids, surrounded by intergranular facets of softened boundaries. The intergranular facets were characterized by very localized plastic deformation at the grain boundaries, as shown in Figure 21. Such a softening allowed grain boundaries to separate without requiring more normal microvoids to be nucleated and coalesced, and strength during the cooling cycle was reduced.

The cross-sectional optical micrograph (Figure 22b) of the sample that was tensile-loaded during the cooling cycle shows the presence of refined grains at the vicinity of the fracture surface. Dynamic recrystallization during rapid high-temperature tensile loading was highly probable, resulting in the observed grain refinement. Commonly, large deformations are necessary before dynamic recrystallization occurs. Recrystallization must have occurred prior to the intergranular separation mentioned above.

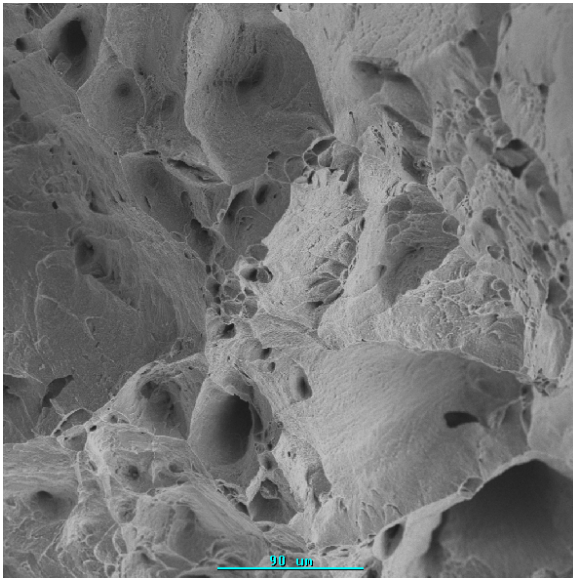


Figure 20. SEM fractograph of as-received HR-160 alloys, tensile-loaded at 1000 C during heating.

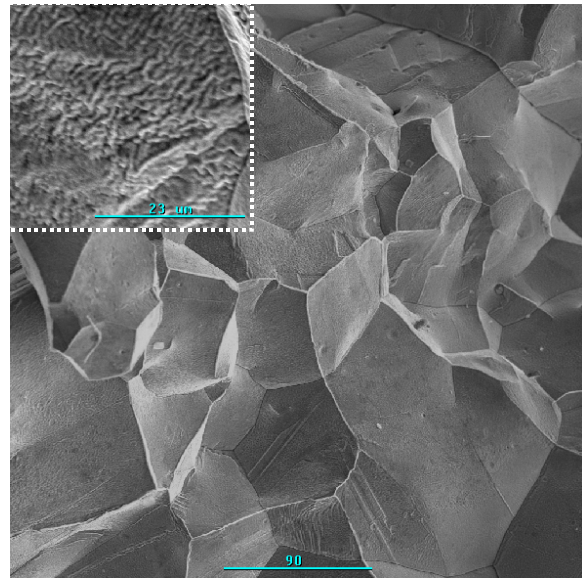


Figure 21. SEM fractograph of as-received HR-160 alloys, tensile-loaded at the peak temperature.

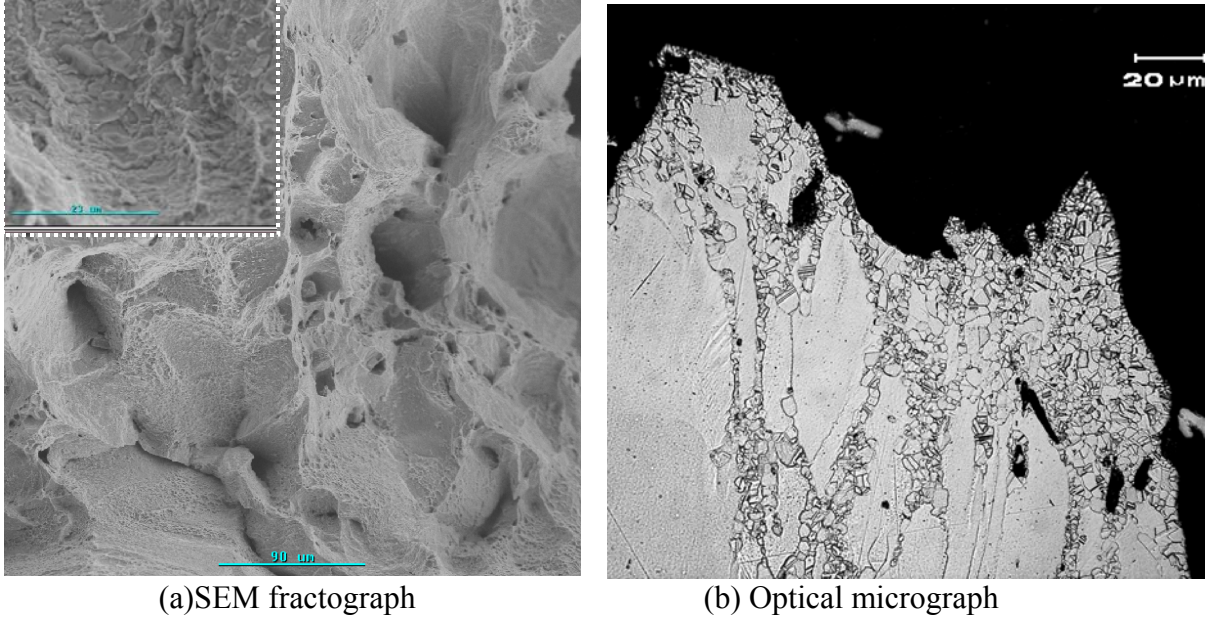
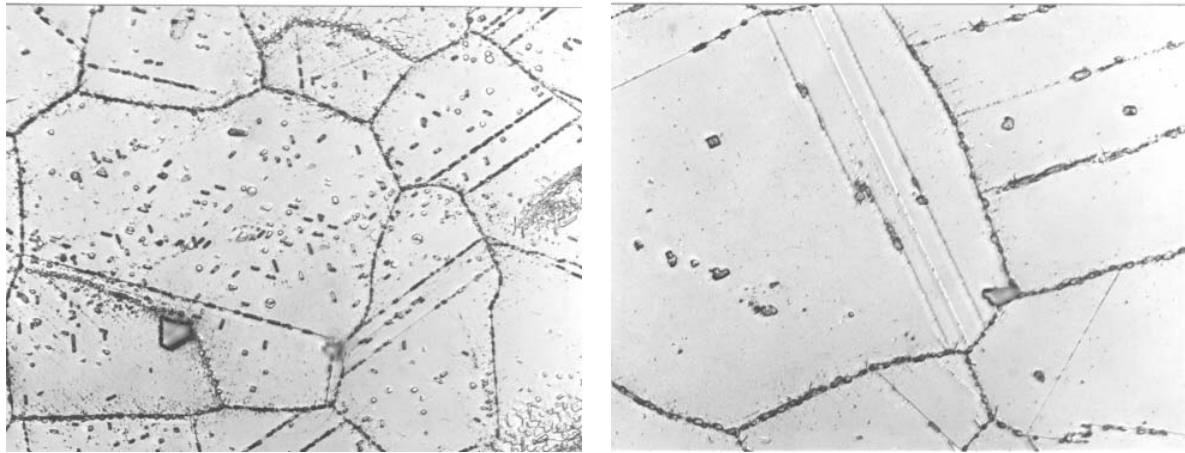


Figure 22. SEM fractograph and optical cross-sectional micrograph of as-received HR-160 alloys, tensile-loaded at 1000 C during cooling, after a heating cycle to the peak temperature.

### 2.3. Hot Ductility Study of the Artificially-Aged Commercial HR-160 alloy

The microstructures of the commercial HR-160 alloys, aged at 760 C and at 870 C for 4000 hrs, are shown in Figure 23a and 23b, respectively. The grain boundaries and twin boundaries are decorated with spherical precipitates. Intragranular precipitation of needle-like precipitates is also evident, particularly in the alloy aged at 760 C. The as-received HR-160 alloy does not contain the precipitates seen in the aged alloy. Haynes International performed material characterization of the aged HR-160 alloys through energy dispersive spectroscopy (EDS) and X-ray diffraction (XRD) of chemically extracted inclusions and precipitates from the matrix. The plate-like precipitates were not easily observed in the optical micrograph. The assessed chemical composition indicated an enrichment of silicon, titanium, chromium, cobalt, and nickel in the groups of precipitates. The precipitates were thought to be the silicon-rich G phase  $[(\text{Ni}, \text{Co})_{16}(\text{Ti}, \text{Cr})_6(\text{Si})_7]$  and  $\text{Cr}_{23}\text{C}_6$  carbides.

To further characterize the precipitates, X-ray diffraction analysis was performed for structural identification. Figure 24 shows the X-ray diffraction analyses of two aged commercial alloys, along with reference patterns of both the G-phase and the  $\text{Cr}_{23}\text{C}_6$  carbide. The locations of the peaks match well with the reference patterns. The only discrepancy is that the relative height of the collected patterns did not show the same peak ratios as those in the reference pattern for  $\text{Cr}_{23}\text{C}_6$  carbide. However, the locations of the peaks are considered sufficient to identify the phases, and variations in the height could be accounted for by measuring variables or by differences in the sample morphologies between the extracted and the reference samples.



(a) Aged at 760 C for 4000 hrs

(b) Aged at 870 C for 4000 hrs.

Figure 23. Optical micrographs of commercial HR-160 alloys, artificially aged.

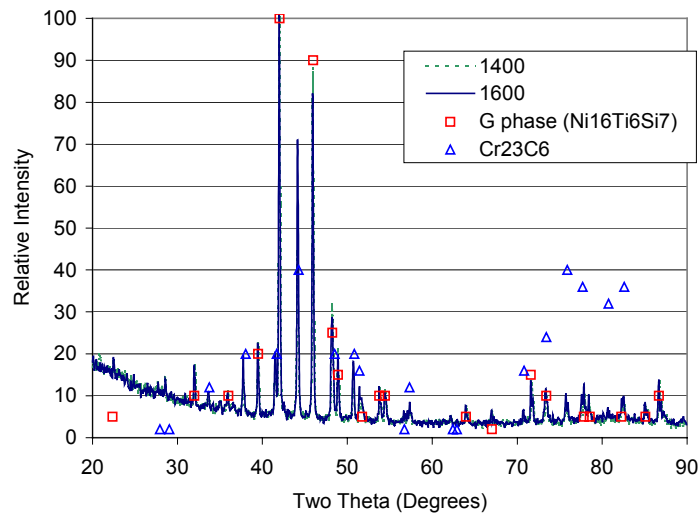


Figure 24. X-ray diffraction of extracted phases from the commercial HR-160 alloy, aged at 760 C and 870 C for 4000 hrs. The actual data, shown as continuous lines, is plotted along with the reference patterns (represented by symbols).

The Gleeble hot ductility response of the aged commercial HR-160 alloy aged at 760 C is shown in Figure 25, while that of the alloy aged at 870 C is shown in Figure 26. As compared to the hot ductility response of the as-received commercial HR-160 alloy (Figure 19), the hot ductility in the aged alloys was significantly compromised, particularly with respect to lower NST temperatures for the aged alloys.

The hot ductility of HR-160 alloy aged at 760 C, shown in Figure 25a, has a NST temperature of 1175 C, which was followed with a quick recover of ductility. However, there was an apparent reduction of ductility observed at 900 C. The limited samples available prevented the investigators from testing at lower temperatures to determine if this drop was actually an indication of the phenomenon known as the ductility dip. For a true ductility dip, the value of reduction of area should increase again at a lower testing temperature. The engineering fracture stresses shown in Figure 25b appeared to continuously decrease during heating or increase during cooling, with a change in slope for each direction of test. This change of slope reflected the change of fracture mechanism at a temperature around 1100 C. The stress values for both the heating and the cooling cycles appeared to be almost identical. Considering the reduction of ductility at 900 C, the identical values between the on-heating and on-cooling engineering fracture stresses at this temperature suggested that such a drop in ductility was not associated with the precipitation hardening in the 760 C aged alloy during the test.

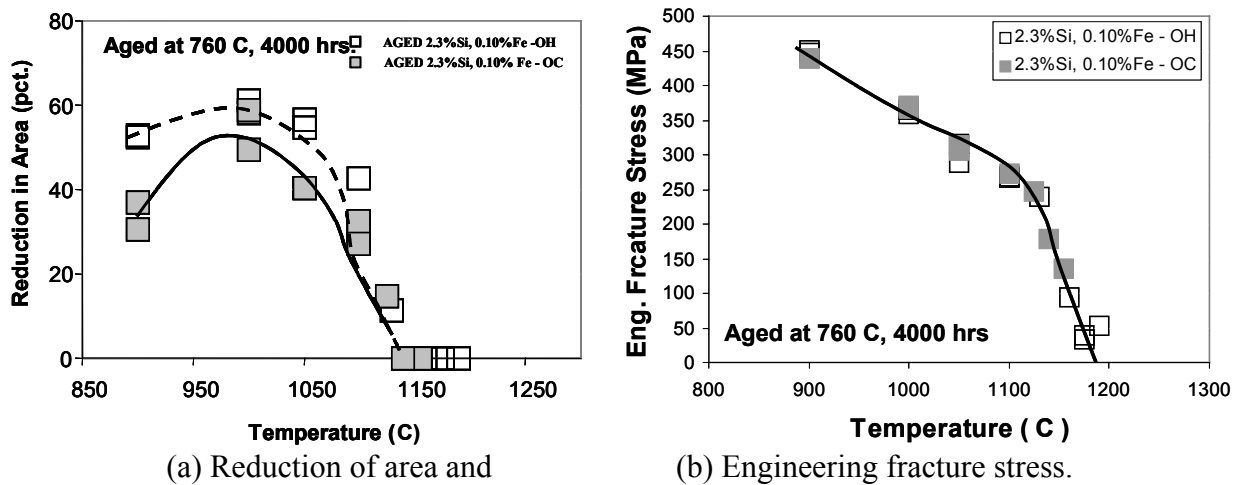


Figure 25. Gleeble hot ductility data for commercial HR-160 alloy, aged at 760 C for 4000 hrs.

In opposition to the result observed from the alloy aged at 760 C, the results for the alloy aged at 870 C, as shown in Figure 26a, indicated a poorer ductility recovery at the vicinity of the NST temperature, but a better ductility at lower temperatures. The zero ductility recovery was approximately 25 C below the alloy's NST of 1165 C. The ductility completely recovered at approximately 1000 C. This recovery was maintained even at the lower temperature of 900 C. The corresponding engineering fracture stresses, in Figure 26b, followed the same trend as the fracture for the alloy aged at 760 C, except that there was an apparent delayed recovery of on-cooling fracture stress which only reconciled with the on-heating values after cooling below 1050 C.

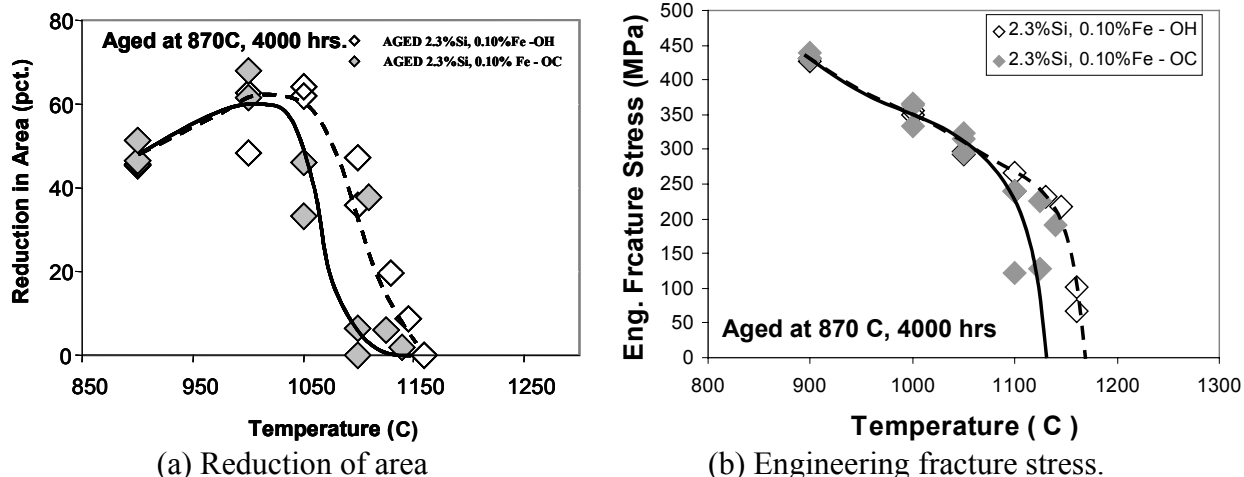
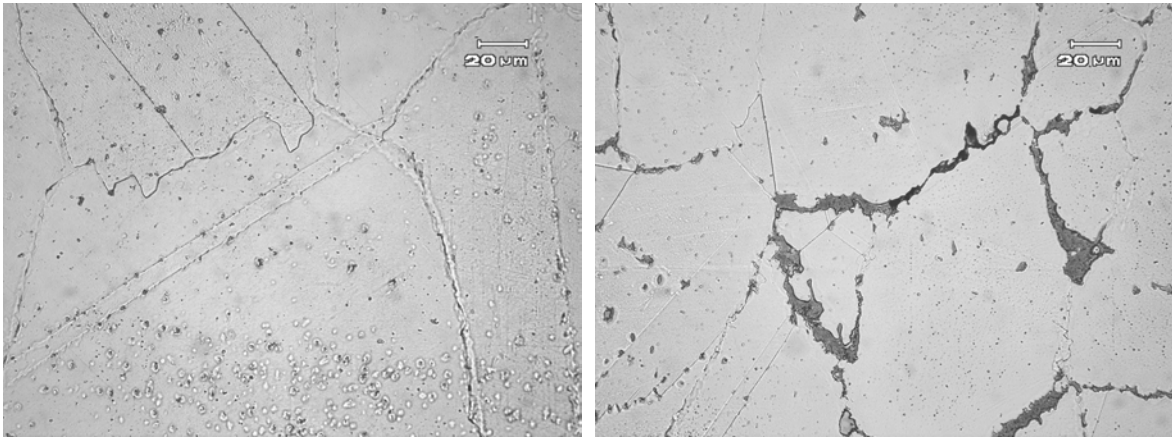


Figure 26. Gleeble hot ductility data for commercial HR-160 alloy, aged at 870 C for 4000 hrs.

The following paragraphs compare fractographs and cross-sectional optical micrographs of selected samples for both aged alloys. An additional test was undertaken to prepare microstructures associated with the simulated HAZ thermal cycles, but free of deformation resulting from rapid tensile loading. A Gleeble thermal processing was completed using heating and cooling cycles identical to those used in the hot ductility testing, but this specimen was quenched by helium without tensile loading. This test was expected to better elucidate the change of microstructures caused by the thermal cycles, just prior to the tensile loading. Regular Gleeble specimens were subjected to significant thermal history subsequent to the fracture process; this was conjectured to promote the formation of additional precipitates in the highly deformed material. Also, brittle phases potentially formed during the thermal cycles could be overlooked at the fracture surface. Examples of these thermally cycled microstructures are those heat-cycled to their corresponding peak temperatures, as shown in Figure 27. In both samples, most of the precipitates had been dissolved. Extensive grain boundary liquation in the alloy aged at 870 C is clearly shown in Figure 27b. On the other hand, only grain boundary migration is apparent in the alloy aged at 760 C.

The following comparison of fractographs and micrographs for the two aged alloys focuses only on the samples subjected to fully simulated HAZ thermal cycles (loaded during cooling cycles). While interesting fracture morphologies were observed from heat-cycled-only samples, they will not be discussed, because fracture during heating is unlikely during practical welding.



(a) Aged at 760 C for 4000 hrs

(b) Aged at 870 C for 4000 hrs.

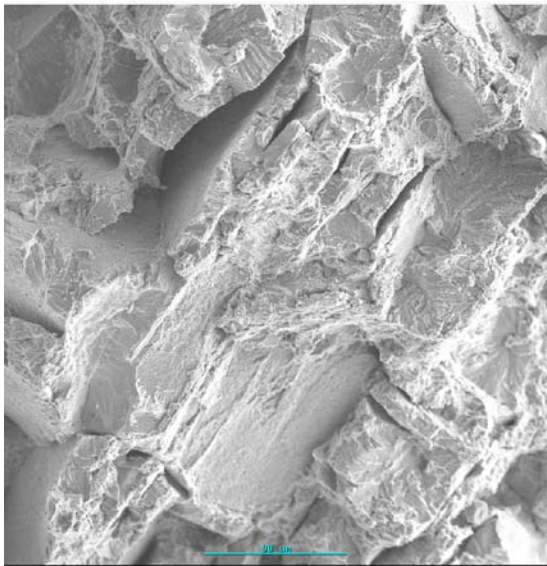
Figure 27. Optical cross-sectional micrographs of commercial HR-160 alloys, helium-quenched at the peak temperature.

- a. Hot ductility at 1100 C [tensile loaded during the cooling cycle after a heating cycle to peak temperature]

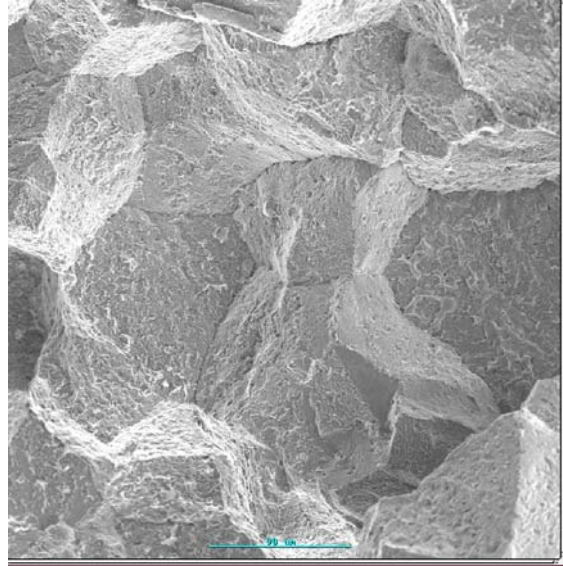
Figure 28 and Figure 29 show the fractographs and the optical micrographs of the hot ductility samples, when tensile loaded at 1100 C during the cooling cycle. Limited evidence of ductility was observed for the alloy aged at 760 C (Figure 28a). Numerous facets were found on the fracture surface, and these facets resembled internal boundaries rather than grain boundaries. Such a condition, where internal boundaries are weaker than the grain boundaries, is not completely understood. Grain boundary liquation is evident on the fracture surface of the alloy aged at 870 C (Figure 28b). The liquefied grain boundaries were significantly undercooled, as reflected by evidence of viscoplastic deformation on the intergranular facets.

The cross-sectional optical micrographs of the two aged alloys (Figures 29a and 29b) indicated limited plastic deformation, in particular for the alloy aged at 870 C. Negligible grain refinement resulting from dynamic recrystallization was observed in the sample aged at 760 C. These observations imply that the weakening of the internal boundaries of the sample aged at 760 C was a deterioration inherently due to the thermal cycle, and was not a consequence of the rapid tensile loading imposed during this test. Therefore, such a boundary weakening may be a real problem in the actual welding construction. In fact, similar facets resembling internal boundaries were also observed, although less frequently, on the fracture surface of samples aged at 870 C, after tensile loading during heating to 900 C. It might be that microstructural evolution of the alloy aged at 760 C reached a condition similar to that of the untested alloy aged at 870 C during the course of the simulated HAZ thermal cycles. Then, the alloy aged at 760 C suffered an elevated temperature embrittlement during the cooling cycle, while the samples aged at 870 C experienced similar problems, but earlier, during the heating cycle.

As shown in Figure 30, the thermally processed samples aged at 760 C produced a microstructure with minor evidence of prior grain boundary liquation. In contrast, a significant amount of grain boundary liquation in the sample aged at 870 C appeared to have been retained during the cooling cycle. As in the samples thermally processed up to the peak temperature (Figure 27), an almost complete dissolution of the previously identified precipitates took place, particularly inside the grains of both alloys.

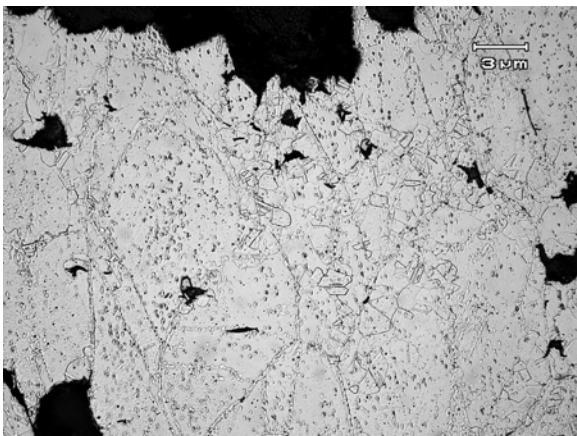


(a) Aged at 760 C for 4000 hrs

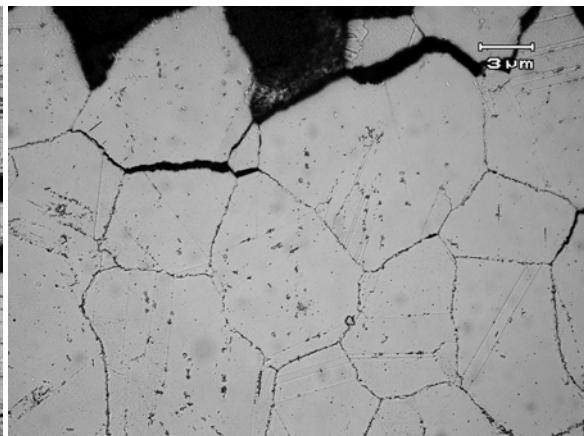


(b) Aged at 870 C for 4000 hrs.

Figure 28. SEM Fractographs of commercial HR-160 alloys, tensile loaded at 1100 C during cooling, after a heating cycle to peak temperature.



(a) Aged at 760 C for 4000 hrs



(b) Aged at 870 C for 4000 hrs.

Figure 29. Optical cross-sectional micrographs of commercial HR-160 alloys, tensile loaded at 1100 C during cooling, after a heating cycle to peak temperature.

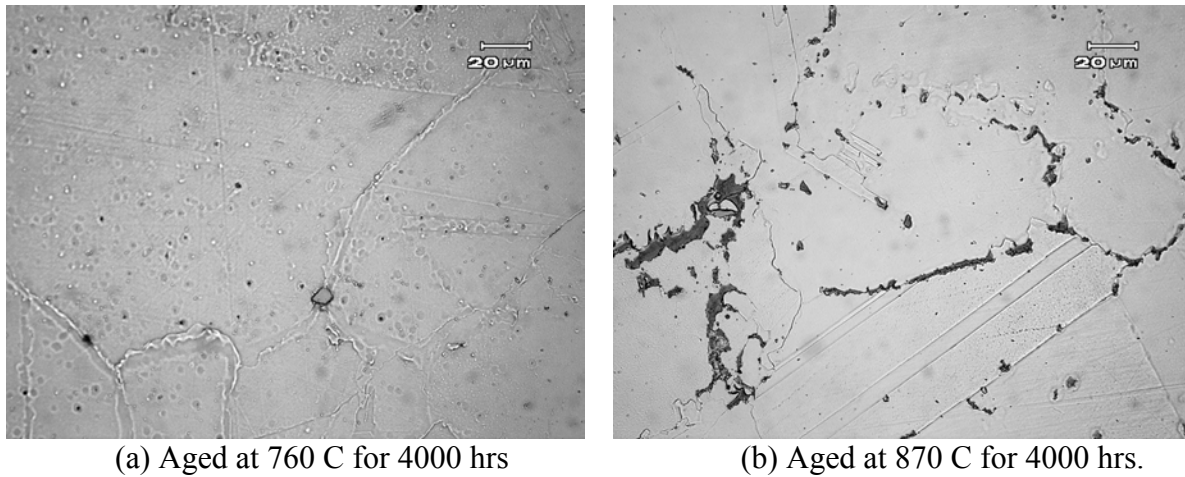


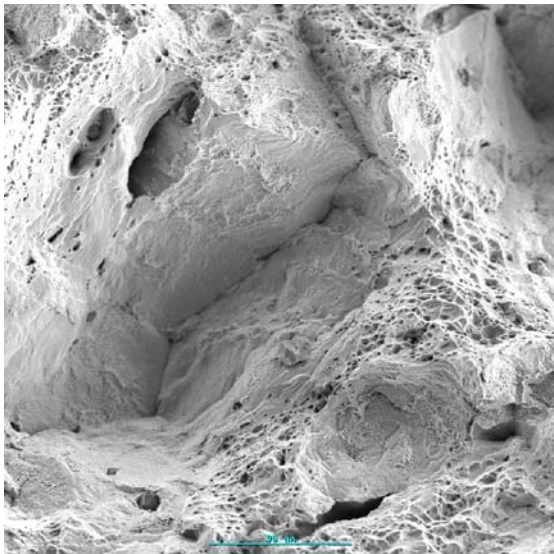
Figure 30. Optical cross-sectional micrographs of commercial HR-160 alloys, helium quenched at 1100 during cooling, after a heating cycle to peak temperature.

- b. Hot ductility at 900 C [tensile loaded during the cooling cycle after a heating cycle to peak temperature]

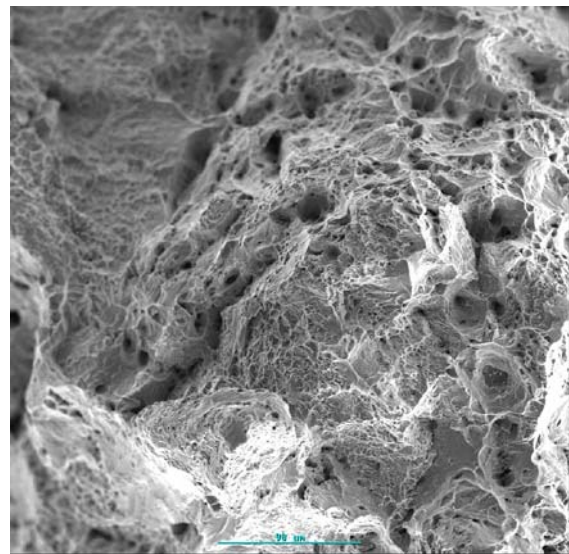
The fracture appearances of the two aged samples, tensile loaded at 900 C during the cooling cycle (after a heating cycle to peak temperature), are shown in Figure 31. Intergranular facets are readily observed on the fracture surface of the sample aged at 760 C, while coalesced microvoids were the dominant fracture feature of the sample aged at 870 C. Closer inspection of the intergranular facets of the sample aged at 760 C showed evidence of viscoplastic deformation associated with grain boundary softening, such as that observed previously in Figure 22a. As was observed for the as-received alloy, significant dynamic recrystallization took place in the sample aged at 760 C. Slip lines were also evident, implying that the recrystallization in the 760 C aged sample was not as complete as that in the as-received sample. The two observations (from the as-received and the samples aged at 870 C, tensile-loaded during the cooling cycle at lower temperatures) appeared to be consistent, and suggested that dynamic recrystallization might be related to the grain boundary softening. Recall that the predominant fracture morphology from the sample aged at 760 C, then tensile-loaded at 1100 C during the cooling cycle, contained facets that resembled internal boundaries. Hence, grain softening in the alloy aged at 760 C would not be expected at a low temperature (such as 900 C), unless localized adiabatic heating occurred.

In contrast to the sample aged at 760 C, insignificant dynamic recrystallization was observed in the sample aged at 870 C. The absence of recrystallization in this sample is consistent with the absence of grain boundary softening. Instead, coalesced microvoids were the predominant fracture feature. The ductile fracture by microvoid coalescence apparently enhanced the ductility of this sample as compared to that of the sample aged at 760 C. The cause of negligible dynamic recrystallization in the sample aged at 870 C has not been further investigated.

The micrographs of the corresponding thermally processed samples are shown in Figure 33. There is nothing particular in the sample aged at 760 C that can be used as a clue to the ease in activation of dynamic recrystallization at 900 C, except that most of the alloying elements are back into the solution. Similarly for the sample aged at 870 C, the microstructure reveals nothing that explains the lack of dynamic recrystallization in this sample. It is also surprising to observe a significant fraction of retained grain boundary liquid in the sample aged at 870 C, yet to measure a higher value of ductility than that found for the sample aged at 760 C.

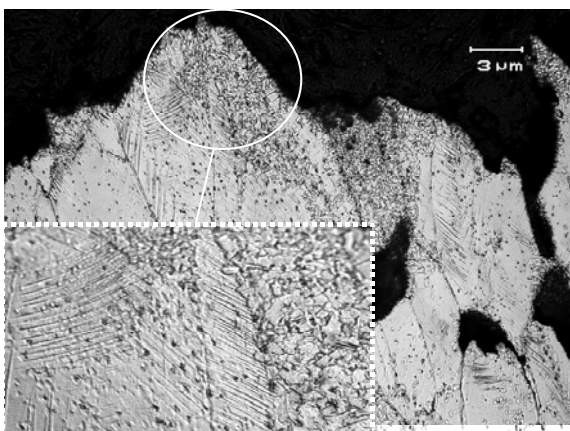


(a) Aged at 760 C for 4000 hrs

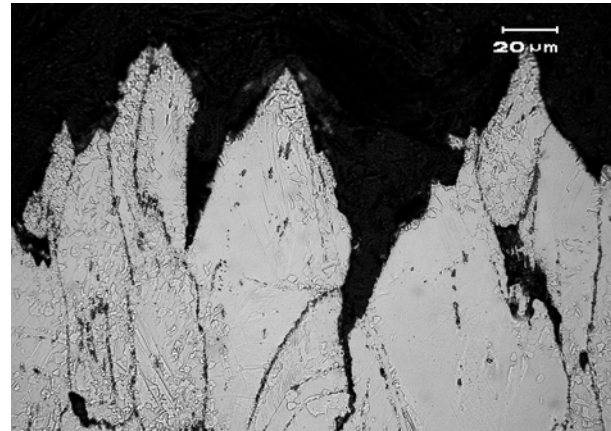


(b) Aged at 870 C for 4000 hrs.

Figure 31. SEM Fractographs of commercial HR-160 alloys, tensile-loaded at 900 C during cooling, after a heating cycle to peak temperature.

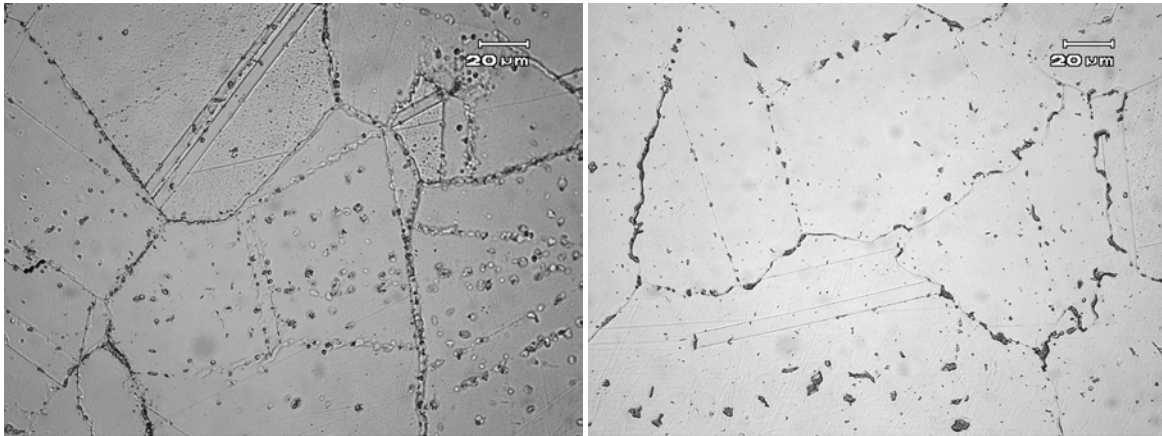


(a) Aged at 760 C for 4000 hrs



(b) Aged at 870 C for 4000 hrs.

Figure 32. Optical cross-sectional micrographs of commercial HR-160 alloys, tensile-loaded at 1100 C during cooling, after a heating cycle to peak temperature.



(a) Aged at 760 C for 4000 hrs

(b) Aged at 870 C for 4000 hrs.

Figure 33. Optical cross-sectional micrographs of commercial HR-160 alloys, helium-quenched at 1100 during cooling, after a heating cycle to peak temperature.

## 2.4. Discussion

In general, the hot ductility responses of the two artificially aged alloys (at 760 C and at 870 C for 4000 hrs) were inferior to that of the as-received alloy. Both alloys had NST temperatures at least 65 C lower than that of the as-received alloy. The engineering fracture stresses of the three alloys appeared to converge to the same value of approximately 350 Mpa during on-cooling tensile loading at 1000 C.

At lower temperature regions, the ductility of the alloy aged at 870 C recovered to a higher value than that of the alloy aged at 760 C during on-cooling tensile loading at 900 C. On the other hand, in the higher temperature regions, the ductility recovery of the alloy aged at 870 C was inferior to that of the alloy aged at 760 C.

It was understood that the standard Gleeble hot ductility test applies a rapid tensile loading to ensure that the fracture takes place at the temperature of interest during such a dynamic thermal process. The obtained results would be temperature specific, and can then be used to define the brittle temperature range of the HAZ of the material, whenever the ductility values are low. However, the rapid tensile loading applied during the Gleeble hot ductility test raises a concern that the dynamic recrystallization in some of the alloys (although unique to the microstructure and composition of the alloy) was not relevant to real welding problems that do not involve such rapid straining. Therefore, the grain boundary softening and the corresponding reduction of ductility values may lead to an incorrect conclusion regarding the HAZ cracking susceptibility of the material. Large, broadly distributed deformations do not occur in actual weld joints; and hence, the large values of reduction in area obtained by this testing are not relevant. On the other hand, results with small values of reduction in area

should be more meaningful for use as a comparison of alloys. Hence, conclusions from the alloys of interest will be drawn from comparison at the high temperature regions only. With this criterion, the alloy aged at 760 C can be considered to be in a better condition for repair welding than the alloy aged at 870 C, while the as-received alloy possesses the superior microstructure.

## **2.5. Conclusions**

1. The aging at both 760 C and 870 C for 4000 hours reduced the hot ductility response, which is believed to increase the HAZ hot cracking susceptibility of the commercial HR-160 alloy.
2. The aging at 760 C produced an alloy with a better condition for repair welding than aging at 870 C.
3. The alloy aged at 870 C is believed to display the most susceptibility to HAZ cracking during repair welding due to the slow recovery of its hot ductility during the cooling cycle.

## **3. References**

1. J.N. DuPont, J.R. Micheal, and B.D. Newbury, *Welding Journal*, 81, 408-415s (1999).
  2. J.N. Dupont, *J. Materials Science*, 32, 4101-4107 (1997).
  3. C.D. Lundin, C.Y.P. Qiao, C.H. Lee, *Weldability of Materials (Proc. Of Materials Weldability Symposium)*, 9-21, ASM International, Materials Park, Ohio, 1990.
  4. C.D. Lundin, C.Y.P. Qiao, T.P.S. Gill, and G.M. Goodwin, *Welding Journal*, 74, 189-200s (1993).
  5. J.N. Dupont, C.V. Rubino, and A.R. Marder, *Welding Journal*, 80 (1998).
  6. Z. Feng, T. Zacharia, and S.A. david, *Welding Journal*, 79, pp. 470-483s (1997).
-